NUREG/CR-
ORNL/TM-2000/321

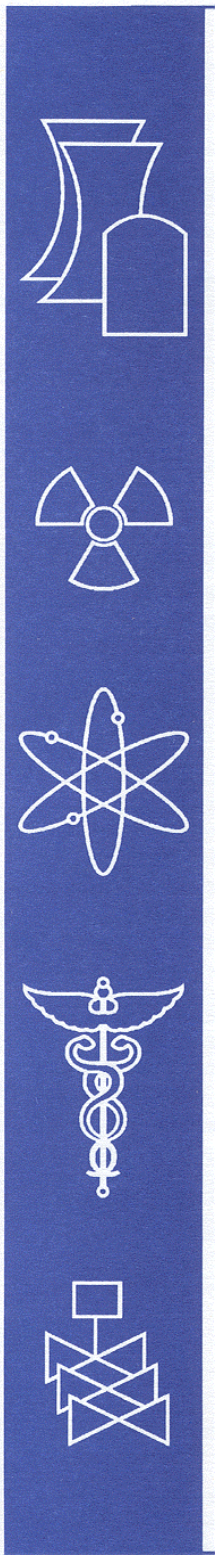

Impact of Integral Burnable Absorbers on PWR Burnup Credit Criticality Safety Analysis for Dry Cask Storage and Transport

Prepared by
C. E. Sanders and J. C. Wagner, ORNL

Oak Ridge National Laboratory

U.S. Nuclear Regulatory Commission
Office of Nuclear Regulatory Research
Washington, DC 20555-0001

AVAILABILITY OF REFERENCE MATERIALS IN NRC PUBLICATIONS

NRC Reference Material

As of November 1999, you may electronically access NUREG-series publications and other NRC records at NRC=s Public Electronic Reading Room at www.nrc.gov.NRC/ADAMS/index.html. Publicly released records include, to name a few, NUREG-series publications; *Federal Register* notices; applicant, licensee, and vendor documents and correspondence; NRC correspondence and internal memoranda; bulletins and information notices; inspection and investigative reports; licensee event reports; and Commission papers and their attachments.

NRC publications in the NUREG series, NRC regulations, and *Title 10, Energy*, of the Code of *Federal Regulations*, may also be purchased from one of these two sources:

1. The Superintendent of Documents
   U.S. Government Printing Office
   P.O. Box 37082
   Washington, DC 20402B9328
   www.access.gpo.gov/su_docs
   202B512B1800
2. The National Technical Information Service
   Springfield, VA 22161B0002
   www.ntis.gov
   1B800B553B6847 or, locally, 703B605B6000

A single copy of each NRC draft report for comment is available free, to the extent of supply, upon written request as follows:

Address: Office of the Chief Information Officer,
Reproduction and Distribution
Services Section
U.S. Nuclear Regulatory Commission
Washington, DC 20555B0001
E-mail: DISTRIBUTION@nrc.gov
Facsimile: 301B415B2289

Some publications in the NUREG series that are

Non-NRC Reference Material

Documents available from public and special technical libraries include all open literature items, such as books, journal articles, and transactions, *Federal Register* notices, Federal and State legislation, and congressional reports. Such documents as theses, dissertations, foreign reports and translations, and non-NRC conference proceedings may be purchased from their sponsoring organization.

Copies of industry codes and standards used in a substantive manner in the NRC regulatory process are maintained atC

The NRC Technical Library
Two White Flint North
11545 Rockville Pike
Rockville, MD 20852B2738

These standards are available in the library for reference use by the public. Codes and standards are usually copyrighted and may be purchased from the originating organization or, if they are American National Standards, fromC

American National Standards Institute
11 West 42nd Street
New York, NY 10036B8002
www.ansi.org
212B642B4900

The NUREG series comprises (1) technical and administrative reports and books prepared by the staff (NUREG/XXXX) or agency contractors (NUREG/CR-XXXX), (2) proceedings of conferences (NUREG/CP-XXXX), (3) reports resulting from international agreements (NUREG/IA-XXXX), (4) brochures (NUREG/BR-XXXX), and (5) compilations of legal decisions and orders of the Commission and Atomic and Safety Licensing Boards and of Directors' decisions under Section 2.206 of NRC's regulations (NUREG-0750).

DISCLAIMER: This report was prepared as an account of work sponsored by an agency of the U.S. Government. Neither the U.S. Government nor any agency thereof, nor any employee, makes any warranty, expressed or implied, or assumes any legal liability or responsibility for any third party's use, or the results of such use, of any information, apparatus, product, or process disclosed in this publication, or represents that its use by such third party would not infringe privately owned rights.

NUREG/CR–XXXX
ORNL/TM–2000/321

12/8/00 12:00 PM – *D R A F T*

Impact of Integral Burnable Absorbers on PWR Burnup Credit Criticality Safety Analysis for Dry Cask Storage and Transport

Manuscript Completed:
Date Published:

Prepared by
C. E. Sanders and J. C. Wagner, ORNL

Oak Ridge National Laboratory
Managed by UT-Battelle, LLC
Oak Ridge, TN 37831–6370

D. D. Ebert, NRC Project Manager

Prepared for
Division of Systems Analysis and Regulatory Effectiveness
Office of Nuclear Regulatory Research
U.S. Nuclear Regulatory Commission
Washington, DC 20555–0001
NRC Job Code W6479

ABSTRACT

The Interim Staff Guidance on burnup credit issued by the Nuclear Regulatory Commission's Spent Fuel Project Office restricts the use of burnup credit to assemblies that have not used burnable absorbers. This restriction eliminates a large portion of the currently discharged spent fuel assemblies from cask loading, and thus, severely limits the practical usefulness of burnup credit. This report examines the effect of integral burnable absorbers (IBAs) on reactivity to provide technical justification for relaxing the current restriction for dry cask storage and transport, and subsequently, to develop the necessary guidelines for relaxing the current restriction. The effect of IBAs on reactivity for various IBA designs and exposure conditions is shown and discussed. Further, the reactivity effect of IBAs for typical initial fuel enrichment and absorber loadings is quantified as a function of burnup. The report concludes with a discussion on the issues for consideration and preliminary recommendations for inclusion of spent fuel assemblies with IBAs in criticality safety analyses using burnup credit for dry cask storage and transport.

CONTENTS

Page

ABSTRACT iii
LIST OF FIGURES vii
LIST OF TABLES xi
ACKNOWLEDGMENTS xiii

1 INTRODUCTION 1

2 INTEGRAL BURNABLE ABSORBER DESIGNS CONSIDERED 3
2.1 Integral Fuel Burnable Absorbers (IFBAs) 3
2.2 UO_2-Gd_2O_3 Integral Burnable Absorber Rods 3
2.3 UO_2-Er_2O_3 Integral Burnable Absorber Rods 4
2.4 Al_2O_3-B_4C Integral Burnable Absorber Rods 4

3 REACTIVITY EFFECT OF INTEGRAL BURNABLE ABSORBER RODS 5
3.1 Introduction and Background 5
3.2 Code Description 6
3.3 Calculations 7
3.3.1 Integral Fuel Burnable Absorber (IFBA) Rods 7
3.3.1.1 IFBA Analyses for 1.57 mg ^{10}B/inch 8
3.3.1.2 IFBA Analyses for 2.355 mg ^{10}B/inch 17
3.3.2 UO_2-Gd_2O_3 Integral Burnable Absorber Rods 17
3.3.2.1 Combustion Engineering (CE) Designs 20
3.3.2.2 Siemens Designs 27
3.3.3 UO_2-Er_2O_3 Integral Burnable Absorber Rods 37
3.3.4 Al_2O_3-B_4C Integral Burnable Absorber Rods 43
3.3.5 Additional Integral Burnable Absorber Rod Studies 50
3.3.5.1 Variations of Gadolinia Loading and Initial Fuel Enrichment 50
3.3.5.2 Variations of IFBA Loading and Initial Fuel Enrichment 53

4 SUMMARY AND IMPLICATIONS 57

5 RECOMMENDATIONS 59

6 REFERENCES 61

LIST OF FIGURES

Figures **Page**

1 Typical reactivity behavior of PWR fuel with and without IBAs (neutron poisons) present 6

2 HELIOS calculational model of an IFBA case containing 156 IFBA rods 9

3 Fuel rod array (17 × 17) representing the 80 IFBA rod loading pattern 10

4 Comparison of k_{inf} values with IFBA rods present (80 IFBA rods, 3.4 wt % ^{235}U enriched fuel) and without IFBA rods (3.4 wt % ^{235}U enriched fuel) 11

5 Comparison of Δk values as a function of burnup between assemblies with and without IFBA rods (80 IFBA rods) for initial enrichments of 3.4 and 4.4 wt % ^{235}U. Note that the results are also plotted according to the enlarged scale on the right-hand side y-axis for clarity. 12

6 Fuel rod array (17 × 17) representing the 104 IFBA rod loading pattern 13

7 Comparison of Δk values as a function of burnup between assemblies with and without IFBA rods (104 IFBA rods) for initial enrichments of 3.4 and 4.0 wt % ^{235}U. Note that the results are also plotted according to the enlarged scale on the right-hand side y-axis for clarity. 14

8 Fuel rod array (17 × 17) representing the 156 IFBA rod loading pattern 15

9 Comparison of Δk values as a function of burnup between assemblies with and without IFBA rods (156 IFBA rods) for initial enrichments of 4.0 and 4.4 wt % ^{235}U. Note that the results are also plotted according to the enlarged scale on the right-hand side y-axis for clarity. 16

10 Comparison of Δk values as a function of burnup between assemblies with and without IFBA rods, with varied number of IFBA rods and an enrichment of 4.617 wt % ^{235}U. Note that the results are also plotted according to the enlarged scale on the right-hand side y-axis for clarity. 18

11 Comparison of Δk values as a function of burnup between assemblies with and without IFBA rods (104 IFBA rods) for initial enrichments of 4.25 and 4.617 wt % ^{235}U. Note that the results are also plotted according to the enlarged scale on the right-hand side y-axis for clarity. 19

12 Fuel rod array (16 × 16) representing the D and E fuel assemblies loading pattern 21

13 Fuel rod array (16 × 16) representing the D1 and E1 fuel assemblies loading pattern 22

14 Fuel rod array (16 × 16) representing the D2 and E2 fuel assemblies loading pattern 23

15 HELIOS calculational model of the D1 fuel assembly containing 8 UO_2-Gd_2O_3 rods 24

LIST OF FIGURES (continued)

Figure **Page**

16 Comparison of Δk values as a function of burnup between the D assembly designs with gadolinia-bearing rods and the D assembly design (Figure 12) without gadolinia-bearing rods. Note that the results are also plotted according to the enlarged scale on the right-hand side y-axis for clarity. 25

17 Comparison of Δk values as a function of burnup between the E assembly designs with gadolinia-bearing rods and the E assembly design (Figure 12) without gadolinia bearing rods. Note that the results are also plotted according to the enlarged scale on the right-hand side y-axis for clarity. 26

18 HELIOS calculational model of M1 fuel assembly 28

19 Fuel rod array (17×17) representing the M1 loading pattern 30

20 Fuel rod array (17×17) representing the M2 loading pattern 31

21 Fuel rod array (17×17) representing the M3 loading pattern 32

22 Fuel rod array (17×17) representing the M4 loading pattern 33

23 Comparison of k_{inf} values with and without gadolinia-bearing rods present (M1 assembly)..... 34

24 Comparison of Δk values as a function of burnup between assemblies with (M1 and M2) and without gadolinia-bearing integral burnable absorber rods. Note that the results are also plotted according to the enlarged scale on the right-hand side y-axis for clarity. 35

25 Comparison of Δk values as a function of burnup between assemblies with (M3 and M4) and without gadolinia-bearing integral burnable absorber rods. Note that the results are also plotted according to the enlarged scale on the right-hand side y-axis for clarity. 36

26 HELIOS calculational model of a fuel assembly containing 60 erbia-bearing fuel rods..... 38

27 Fuel rod array (14×14) representing the 20 UO_2-Er_2O_3 rod loading pattern..... 39

28 Fuel rod array (14×14) representing the 60 UO_2-Er_2O_3 rod loading pattern..... 40

29 Comparison of k_{inf} values with Er_2O_3 integral burnable absorber rods present (assembly with 60 Er_2O_3 integral burnable absorber rods) and without Er_2O_3 integral burnable absorber rods present..... 41

30 Comparison of Δk values as a function of burnup between assemblies with and without Er_2O_3 fue rods present. The fuel rods have a ^{235}U enrichment of 4.3 wt % and the Er_2O_3 integral burnable absorber rods contain 2.0 wt % erbia. Note that the results are also plotted according to the enlarged scale on the right-hand side y-axis for clarity. 42

LIST OF FIGURES (continued)

Figure **Page**

31 HELIOS calculational model of a fuel assembly containing 12 Al_2O_3-B_4C rods 44

32 Fuel rod array (14 × 14) representing the 4 Al_2O_3-B_4C rod loading pattern 45

33 Fuel rod array (14 × 14) representing the 8 Al_2O_3-B_4C rod loading pattern 46

34 Fuel rod array (14 × 14) representing the 12 Al_2O_3-B_4C rod loading pattern 47

35 Comparison of k_{inf} values with (12 B_4C rods) and without B_4C integral burnable absorber rods present 48

36 Comparison of Δk values as a function of burnup between assemblies with and without Al_2O_3-B_4C rods present. The fuel rods have a ^{235}U enrichment of 4 wt % and the Al_2O_3-B_4C integral burnable absorber rods have 4 wt % B_4C. 49

37 Comparison of Δk values versus burnup with varying gadolinia weight percents. The fuel enrichments are 3.78/3.28 wt % ^{235}U. 51

38 Comparison of Δk values versus burnup with various ^{235}U enrichments. The eight integral burnable absorber rods have 6 wt % Gd_2O_3. 52

39 Comparison of Δk values versus burnup with varying IFBA loadings. The ^{235}U enrichment is 4 wt % for all cases. 53

40 Comparison of Δk values versus burnup with the 32 IFBA loading pattern showing varying ^{235}U enrichments. Note that the results are also plotted on the enlarged scale on the right-hand side y-axis for clarity. 54

41 Comparison of Δk values versus burnup with the 156 IFBA loading pattern showing varying ^{235}U enrichments. Note that the results are also plotted on the enlarged scale on the right-hand side y-axis for clarity. 55

LIST OF TABLES

Table		Page
1	Summary of parameters used for the depletion calculations	7
2	Westinghouse 17 × 17 fuel assembly specifications	8
3	CE 16 × 16 fuel assembly specifications	20
4	Fuel assembly data for the D and E sets of assembly designs	20
5	Siemens 17 × 17 fuel assembly specifications	27
6	Fuel assembly data for the M1–M4 assembly designs	29
7	CE 14 × 14 fuel assembly specifications (Er_2O_3)	37
8	CE 14 × 14 fuel assembly specifications (Al_2O_3-B_4C)	43
9	Summary of maximum positive Δk values observed for IFBA cases	56

ACKNOWLEDGMENTS

1 INTRODUCTION

The concept of taking credit for the reduction in reactivity due to fuel burnup is commonly referred to as *burnup credit*. The reduction in reactivity that occurs with fuel burnup is due to the change in concentration (net reduction) of fissile nuclides and the production of actinide and fission-product neutron absorbers. The change in the concentration of these nuclides with fuel burnup, and consequently the reduction in reactivity, is dependent upon the depletion environment (e.g., the neutron spectrum). Therefore, the utilization of credit for fuel burnup necessitates consideration of a wide range of fuel designs and operating conditions.

Continuing advancements in fuel assembly design have enabled enhanced fuel utilization; thereby increasing the performance of reactor cores (i.e., extending core lifetimes). One characteristic of these advanced fuel assembly designs is the expanded use of burnable absorber (neutron poison) materials, either as an integral part of the fuel assembly or as a separate assembly used in conjunction with the fuel assembly. The burnable absorbers may be classified into two distinct categories: (1) Burnable Poison Rods (BPRs) and (2) Integral Burnable Absorbers (IBAs). BPRs are rods containing neutron-absorbing material that are inserted into the guide tubes of a Pressurized-Water Reactor (PWR) assembly during normal operation and are commonly used for reactivity control and enhanced fuel utilization. In contrast, IBAs refer to burnable poisons that are a nonremovable or integral part of the fuel assembly once it is manufactured. An example of an integral burnable absorber is the Westinghouse Integral Fuel Burnable Absorber (IFBA) rod, which has a coating of zirconium diboride (ZrB_2) on the fuel pellets. IBAs are used extensively in many current PWR fuel assembly designs. Although BPRs are also commonly used in PWRs, this report will focus on the effect of IBAs only. The effect of BPRs are addressed in Ref. 1.

The Interim Staff Guidance[2] on burnup credit issued by the Nuclear Regulatory Commission's Spent Fuel Project Office recommends licensees restrict the use of burnup credit to assemblies that have not used burnable absorbers. This restriction eliminates a large portion of the currently discharged spent fuel assemblies from cask loading, and thus, severely limits the practical usefulness of burnup credit. Therefore this report examines the effect of IBAs on reactivity for various designs and enrichment/poison loading combinations as a function of burnup. All IBA types that have been widely used in United States (U.S) commercial PWRs are included in this evaluation, and to the extent possible, analyses are presented for a realistic range of initial fuel enrichment and poison loading combinations that are representative of actual assemblies. The effects are quantified, and trends with initial fuel enrichment and poison loading are noted. The report concludes with a discussion on the issues for consideration and preliminary recommendations for inclusion of spent fuel assemblies with IBAs in criticality safety analyses using burnup credit for dry cask storage and transport.

2 INTEGRAL BURNABLE ABSORBER DESIGNS CONSIDERED

Several different types of IBAs have been used in commercial nuclear fuel assembly designs. However, all of the various designs are similar in that they contain thermal neutron absorbing material as an integral nonremoval part of the fuel assembly. Variations in the IBA material, composition, placement within rods, and rod configurations exist among current PWR fuel assembly designs. These IBA characteristics may be varied in combination with the initial fuel assembly enrichment and core location to achieve core operating and fuel management goals, resulting in variations among IBA fuel assembly designs. For completeness, analyses are presented in this report for all known (to the authors), unique IBA materials in their corresponding fuel assembly designs. These include Westinghouse assembly designs with IFBAs, Combustion Engineering (CE) and Siemens assembly designs with UO_2-Gd_2O_3 rods, CE assembly designs with UO_2-Er_2O_3 rods, and CE assembly designs with B_4C rods. To the extent possible, analyses are performed for a representative, realistic range of actual fuel initial enrichment and poison loading combinations. For clarity, each of the unique IBA types considered in this report is described below. All IBA types that have been widely used in U.S. commercial PWRs are included in this evaluation.

It cannot, however, be confirmed that all types that have ever been used in U.S. PWRs are included in this evaluation. The fuel assembly design data used for this analysis were collected from a variety of non-proprietary sources. For many of the IBA types, complete, detailed specifications were not openly available in any single document, largely due to fuel vendor's desire to protect design information for commercial reasons. Therefore, the complete fuel design specifications required for this analysis were assembled from multiple sources and are documented in this report for reference.

2.1 INTEGRAL FUEL BURNABLE ABSORBERS (IFBAs)

Some Westinghouse fuel assembly designs include Integral Fuel Burnable Absorber (IFBA) rods, which contain enriched uranium dioxide (UO_2) fuel pellets with a thin coating of zirconium diboride (ZrB_2) on the outer surface. To our knowledge, IFBA rods are exclusive to Westinghouse and have been used in Westinghouse reactor cores since about 1987. Specification of the assembly designs that utilize IFBA rods include the Boron loading in the ZrB_2 coating, the number of IFBA rods, and the placement or loading pattern of the IFBA rods within the fuel assembly. The number of IFBA rods within a fuel assembly may vary from zero to ~60% of the total number of fuel rods. For a Westinghouse 17×17 assembly, which contains 264 fuel rods, loading patterns with 0, 8, 16, 32, 48, 64, 80, 104, 128, and 156 IFBA rods are known to exist. In addition, the boron loading in the ZrB_2 coating and the initial ^{235}U enrichment are varied to meet core management goals.

2.2 UO_2-Gd_2O_3 INTEGRAL BURNABLE ABSORBER RODS

A number of nuclear fuel vendors, including CE, Framatome Cogema Fuels (formerly B&W), and Siemens, have manufactured a gadolinia-uranium (UO_2-Gd_2O_3) integral burnable absorber rod. These UO_2-Gd_2O_3 rods, or gadolinia rods, are fuel rods with gadolinia (Gd_2O_3) as an integral part of the fuel matrix and are also used extensively in Boiling Water Reactors (BWRs). The weight percent or loading of Gd_2O_3 in each gadolinia-bearing rod and the number of gadolinia rods within an assembly are both variable. Further, the ^{235}U enrichment among the gadolinia-bearing and nongadolinia-bearing fuel rods is varied to a small extent in some designs.

2.3 UO_2-Er_2O_3 INTEGRAL BURNABLE ABSORBER RODS

In addition to UO_2-Gd_2O_3 rods, CE has manufactured an integral burnable absorber containing erbia (Er_2O_3). Similar to the UO_2-Gd_2O_3 rods, the erbia rods include the burnable absorber (Er_2O_3) as an integral part of the fuel matrix. The weight percent or loading of the erbia and the number of erbia rods within an assembly are both variable, as well as the ^{235}U enrichment.

2.4 AL_2O_3-B_4C INTEGRAL BURNABLE ABSORBER RODS

Another integral burnable absorber manufactured by CE consists of solid rods containing alumina pellets with uniformly dispersed boron carbide particles (Al_2O_3-B_4C), clad in Zircaloy. Unlike the IFBA, UO_2-Gd_2O_3, and UO_2-Er_2O_3, these rods do not contain fuel. The weight percent of B_4C and the number of rods per assembly are variable. These rods are similar to BPRs, but are classified herein as IBAs because they are an integral nonremoval part of the fuel assembly.

3 REACTIVITY EFFECT OF INTEGRAL BURNABLE ABSORBER RODS

3.1 INTRODUCTION AND BACKGROUND

For PWR fuels without IBAs, the reactivity decreases with burnup in a nearly linear fashion. In contrast, for PWR fuel assembly designs that make significant use of IBAs, the reactivity actually increases as fuel burnup proceeds, reaches a maximum at a burnup where the IBA is nearly depleted, and then decreases with burnup in a nearly linear fashion. For fuel assembly designs that make modest use of IBAs, the reactivity decreases with burnup slowly up to the point where the IBA is nearly depleted, and then decreases with burnup in the nearly linear manner. The assemblies are typically designed such that the burnable absorber is effectively depleted in the first third of the assembly life, and as a result, the assembly reactivity typically peaks within this period of burnup. The reactivity behavior of a PWR fuel assembly with and without IBAs (neutron poisons) present as a function of burnup is illustrated in Figure 1.

The presence of IBAs during depletion hardens the neutron spectrum, resulting in lower ^{235}U depletion and higher production of fissile plutonium isotopes. Enhanced plutonium production and the concurrent diminished fission of ^{235}U due to increased plutonium fission can potentially increase the reactivity of the fuel at discharge and beyond, depending on the IBA assembly design characteristics. However, as mentioned, the assemblies are typically designed such that the burnable absorber is effectively depleted in the first third of the assembly life, and thus is exposed to a hardened spectrum during the first third of its exposure only. Note that, unlike BPRs, which are inserted into assembly guide tubes, IBAs do no displace moderator in the assembly lattice, and thus generally have a less significant impact on the neutron spectrum.

Although a great deal of work has been performed related to IBA designs and development for greater fuel utilization and core performance, studies to assess the significance of IBAs on the reactivity of discharged fuel are minimal. Recent work[3] has provided illustrative examples intended to represent typical magnitudes of the reactivity effects of IBAs, including IFBA, UO_2-Gd_2O_3, and UO_2-Er_2O_3 rods. Although the analyses were limited to a single case for each type of IBA, indications from this study are that the neutron-multiplication factor for an assembly without IBAs is always greater (as a function of burnup) than the neutron-multiplication factor for an assembly that utilized UO_2-Gd_2O_3 or UO_2-Er_2O_3 rods. Conversely, the neutron-multiplication factor for an assembly without IFBA rods was found to be slightly less (~0.2% Δk at target discharge burnup) than the neutron-multiplication factor for an assembly with IFBA rods present. The study concludes that neglecting the IBAs yields conservative results for gadolinia- and erbia-bearing fuel and nonconservative results for IFBA fuel, and that the reactivity effect from IBAs is generally small and well behaved.

The following sections describe the calculational methods used for this evaluation and present detailed analyses to demonstrate the reactivity effect of IBAs as a function of burnup. The analyses include variations in the IBA type, concentration, and initial fuel enrichment.

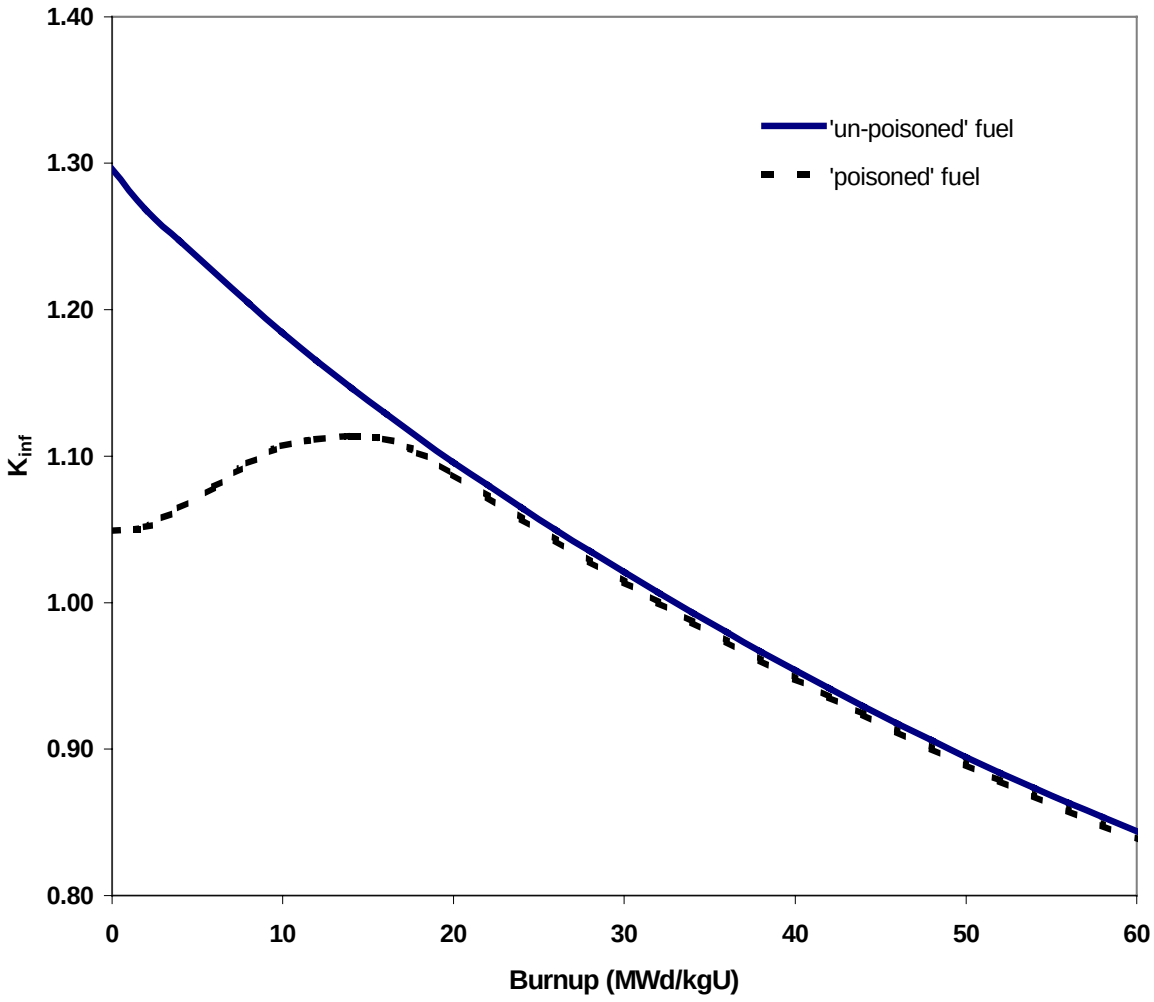

Figure 1 Typical reactivity behavior of PWR fuel with and without IBAs (neutron poisons) present

3.2 CODE DESCRIPTION

The calculations presented in the following sections were performed using the HELIOS-1.6 code package,[4] which primarily consists of three programs: AURORA, HELIOS, and ZENITH. HELIOS is a two-dimensional (2-D), generalized-geometry transport theory code based on the method of collision probabilities with current coupling. AURORA, the input processor, is used to define the geometry, materials, and calculational parameters. ZENITH, the output processor, reads the results saved by HELIOS (in a binary database) and outputs the results in text format. The HELIOS code system also contains the ORION program for viewing and checking model geometries and materials.

HELIOS was employed for this analysis because of its capability to explicitly model the relatively complicated, heterogeneous assembly lattices associated with IBAs. The various structures within each of the assembly models were coupled using angular current discretization (interface currents). All calculations

are for an infinite array of fuel assemblies and utilize the 45-group neutron cross-section library based on ENDF/B-VI.

3.3 CALCULATIONS

Unless specifically stated otherwise, all depletion calculations were performed using the properties and parameters given in Table 1. Using the isotopic compositions from the depletion calculations, branch or restart calculations were performed to determine the neutron-multiplication factor as a function of burnup for out-of-reactor conditions (i.e., 20°C with no soluble boron present) and zero cooling time. In general, for each unique IBA assembly design considered, a calculation was performed for (1) the actual assembly specification (including the presence of the IBA) and (2) an artificial condition in which the IBA was neglected. Throughout the following sections, the Δk values between these two conditions are reported to assess the effect of IBAs on the reactivity of spent nuclear fuel.

Table 1 Summary of parameters used for the depletion calculations

Parameter	Values used in analyses
Moderator temperature (K)	600
Fuel temperature (K)	1000
Fuel density (g/cc)	10.44 (UO_2)
Clad temperature (K)	600
Clad density (g/cc)	5.78 (Zr)
Power density* (MW/t)	60
Moderator boron concentration (ppm)	650

* Various cases were also calculated using a power density of 30 MW/t (which is a more realistic value). The results showed that the Δk values presented in the following sections are not sensitive to variations in the power density.

3.3.1 Integral Fuel Burnable Absorber (IFBA) Rods

The Integral Fuel Burnable Absorber (IFBA), developed by Westinghouse, consists of a thin coating of zirconium diboride (ZrB_2) on the outer surface of the fuel pellets. Various IFBA loading (^{10}B concentration and number of IFBA rods) and enrichment combinations were studied in order to establish the reactivity effect as a function of burnup. The absorber loading and enrichment combinations considered are based on actual fuel assemblies, and were selected to encompass the range of known variations; including number of IFBA rods, ^{10}B concentration, and initial fuel enrichment. All of the IFBA rod analyses were performed with a Westinghouse 17×17 assembly. Dimensional specifications for the fuel assembly are given in Table 2.

Analyses are presented in this section for IFBA assembly designs with 80, 104, and 156 IFBA rods, two different Boron loadings (1.57 and 2.355 mg ^{10}B/inch), and corresponding variations in initial fuel enrichment. With the exception of the loading patterns, the specification of the actual IFBA assembly characteristics (i.e., number of IFBA rods, ^{10}B loading, and initial enrichment) was obtained from Ref. 5. The IFBA loading patterns used in these analyses originated from Ref. 6. Figure 2 displays the geometry of one of the IFBA assemblies (containing 156 IFBA rods) as modeled in HELIOS.

Table 2 Westinghouse 17 × 17 fuel assembly specifications

Parameter	Dimensions (cm)
Rod pitch	1.260
Assembly pitch	21.5
Cladding outside diameter	0.8898
Cladding inside diameter	0.8001
Pellet outside diameter	0.7840
Guide/instrument tube outside diameter	1.204
Guide/instrument tube inside diameter	1.124
Array size	17 × 17
Number of fuel rods	264
Number of guide/instrument tubes	25

The presentation of the IFBA analyses is divided into two subsections, based on the boron loading. The two subsections compare results for linear poison material (boron) loadings of 1.57 and 2.355 mg ^{10}B/inch of pellet, respectively.

3.3.1.1 IFBA Analyses for 1.57 mg ^{10}B/inch

The first IFBA assembly design considered is a 17 × 17 assembly with 80 IFBA rods, as shown in Figure 3. Calculations were performed for (1) the actual assembly specification (as shown in Figure 3) and (2) an artificial condition in which the IFBAs rods were replaced by non-IFBA fuel rods. The k_{inf} values, as a function of burnup from the two calculations, are compared in Figure 4. The Δk values between these two conditions are determined to assess the effect of the IBAs on reactivity.

Separate calculations were performed with enrichments of 3.4 and 4.4 wt % ^{235}U to cover the range of initial enrichments found in the available fuel data[5] for this particular IFBA loading, which consisted of actual fuel assembly data from the Seabrook plant. The results (Δk as a function of burnup) are shown in Figure 5, where it can be seen that both cases achieve a positive Δk (i.e., the k_{inf} value with IFBA rods present becomes greater than the k_{inf} value without IFBA rods present). The Δk for the case with 3.4 wt % ^{235}U enrichment becomes positive (maximum of approximately 0.15%) at a burnup of around 22 MWd/kgU reaching a maximum of approximately 0.15% Δk at around 35 MWd/kgU. The Δk for the case with 4.4 wt % ^{235}U enrichment becomes positive at a burnup of around 28 MWd/kgU with a maximum of 0.15% Δk near 50 MWd/kgU. Consistent with previously published work,[3] these results indicate that the IFBA bearing fuel k_{inf} is not always less than the non-IFBA fuel k_{inf}.

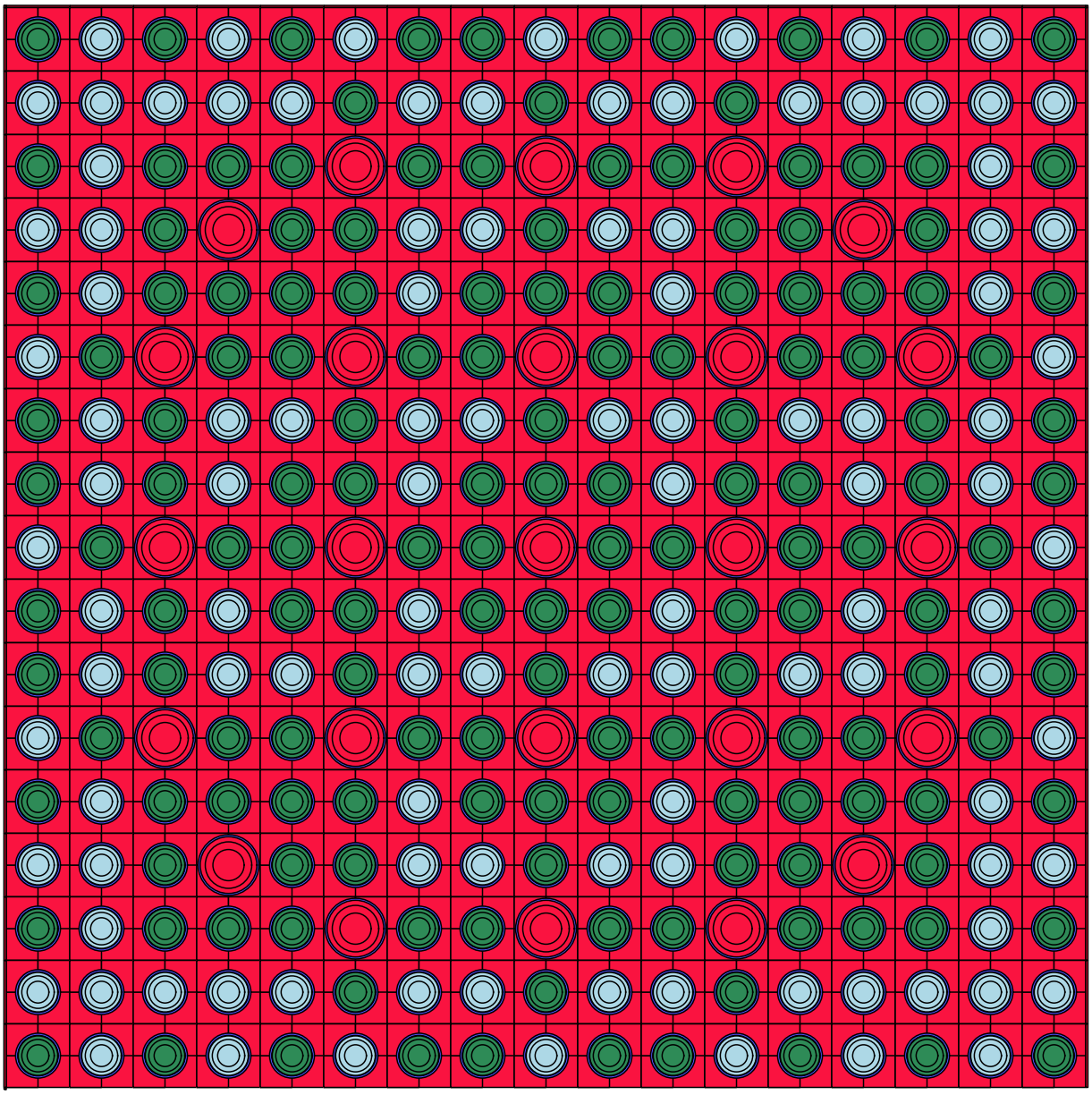

Figure 2 HELIOS calculational model of an IFBA case containing 156 IFBA rods

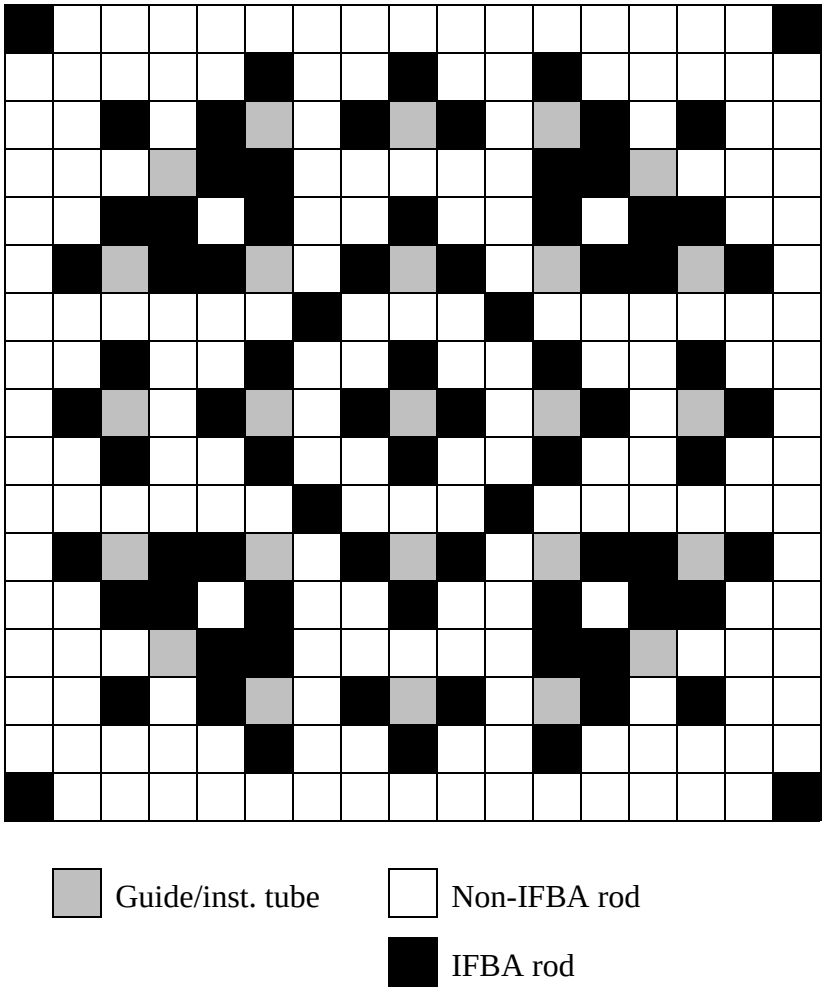

Figure 3 Fuel rod array (17 × 17) representing the 80 IFBA rod loading pattern

The second IFBA design considered contains 104 IFBA rods as shown in Figure 6. As with all designs in this subsection, the poison material loading is 1.57 mg ^{10}B/in. of pellet. Once again, the initial enrichment was varied to span the range within the actual fuel data. The results (Δk as a function of burnup) are shown in Figure 7, where it can be seen that both cases achieve a positive Δk. The Δk values for the case with 3.4 wt % ^{235}U enrichment become positive (maximum of approximately 0.24%) at a burnup of about 22 MWd/kgU reaching a maximum of approximately 0.24% Δk at around 35 MWd/kgU. The Δk for the case with 4.0 wt % ^{235}U enrichment becomes positive (maximum of approximately 0.21%) at a burnup of about 24 MWd/kgU, with a maximum of 0.21% Δk near 50 MWd/kgU. Note that the Δk values reach a maximum and are decreasing with increased burnup beyond that point. Consistent with the results shown for 80 IFBA rods, these results further confirm that an IFBA bearing fuel assembly is not always less than that of a non-IFBA fuel assembly.

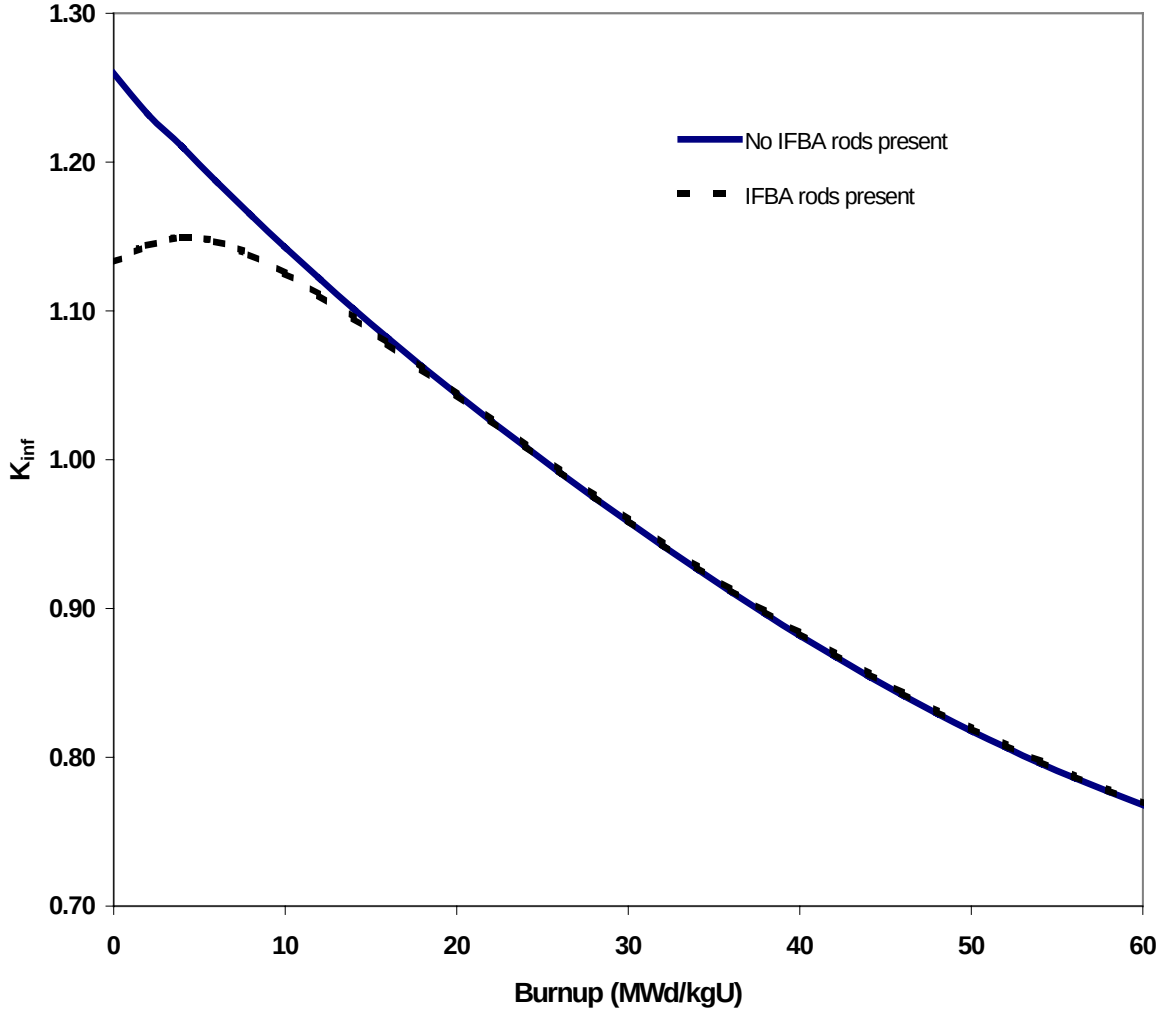

Figure 4 Comparison of k_{inf} values with IFBA rods present (80 IFBA rods, 3.4 wt % ^{235}U enriched fuel) and without IFBA rods (3.4 wt % ^{235}U enriched fuel)

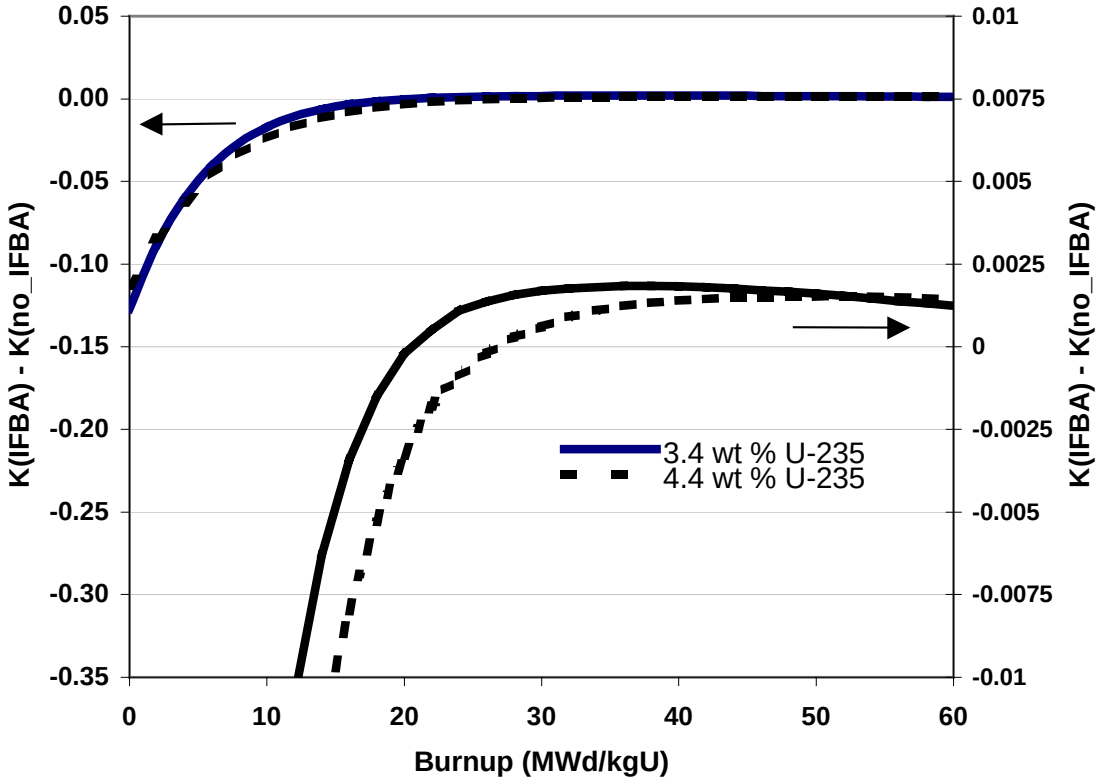

Figure 5 Comparison of Δk values as a function of burnup between assemblies with and without IFBA rods (80 IFBA rods) for initial enrichments of 3.4 and 4.4 wt % ^{235}U. Note that the results are also plotted according to the enlarged scale on the right-hand side y-axis for clarity.

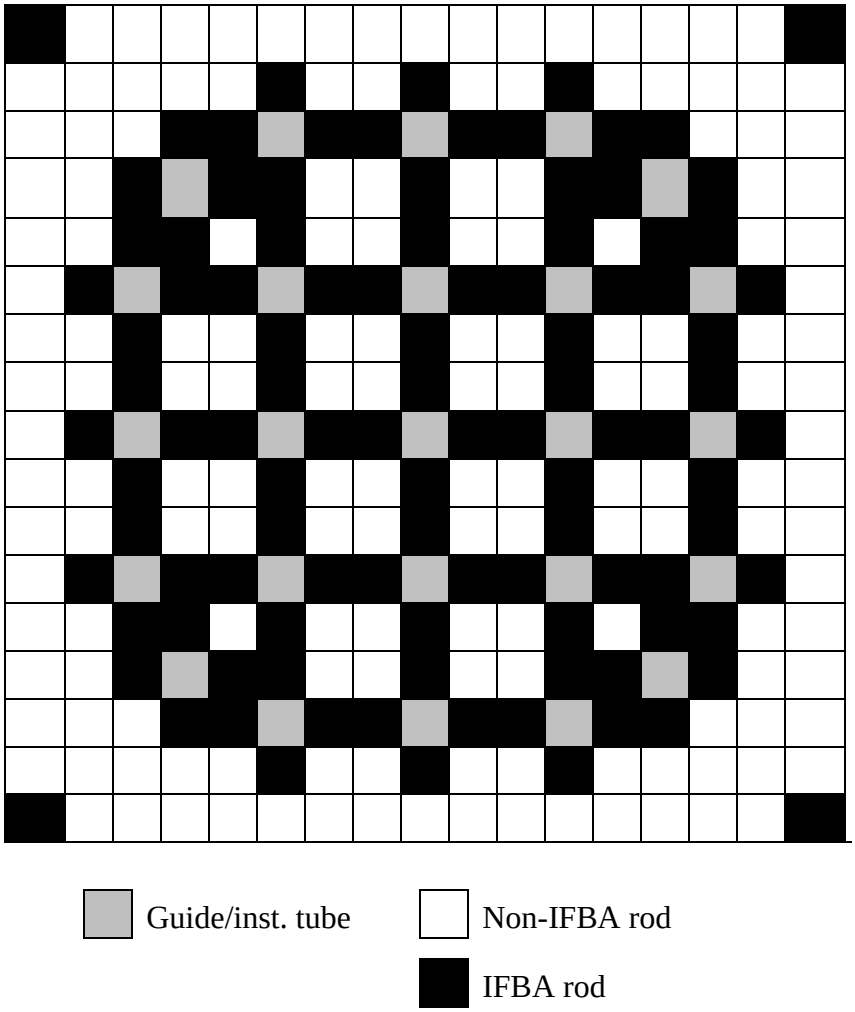

Figure 6 Fuel rod array (17 × 17) representing the 104 IFBA rod loading pattern

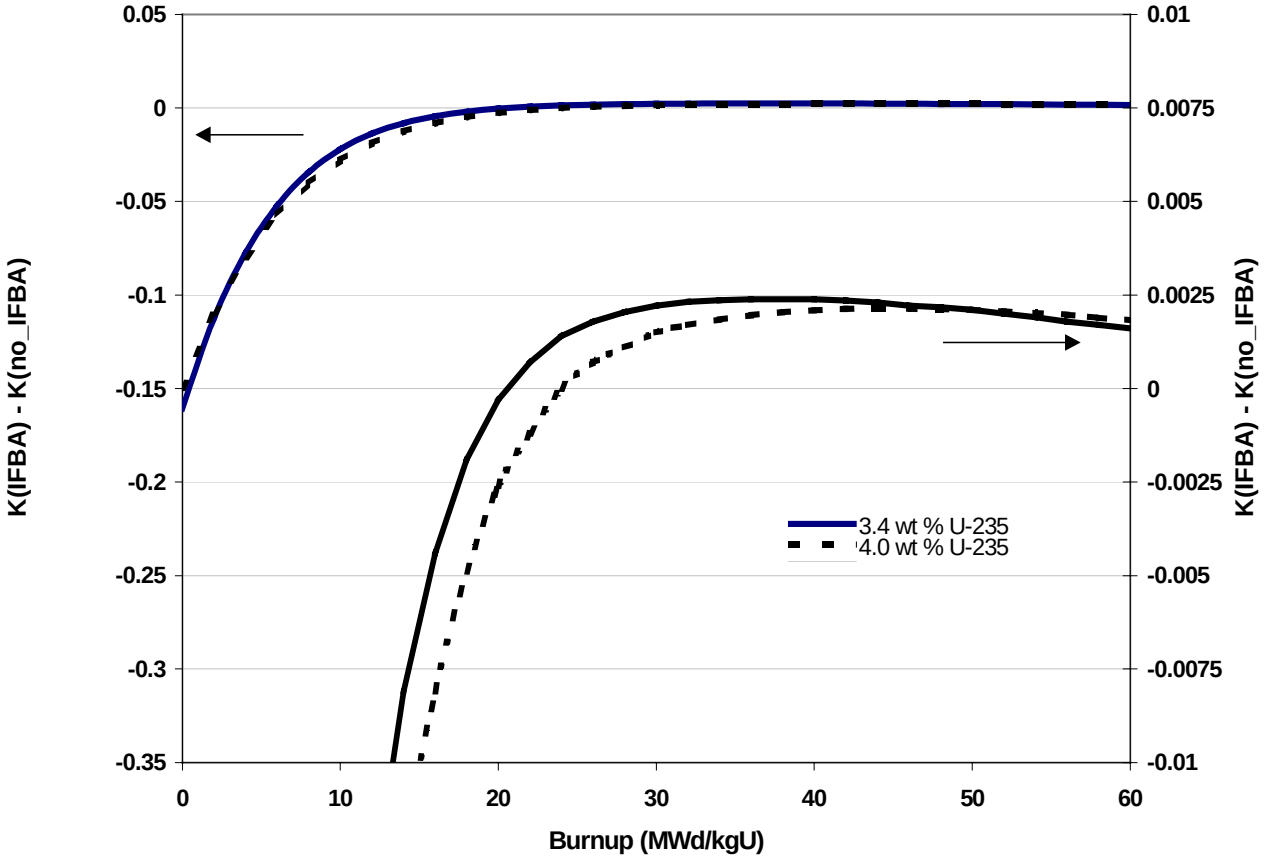

Figure 7 Comparison of Δ*k* values as a function of burnup between assemblies with and without IFBA rods (104 IFBA rods) for initial enrichments of 3.4 and 4.0 wt % ^{235}U. Note that the results are also plotted according to the enlarged scale on the right-hand side y-axis for clarity.

The third and final (for this particular ^{10}B loading) IFBA design considered contains 156 IFBA rods according to Figure 8. Based on actual fuel data, the ^{235}U enrichment was varied between 4.0 and 4.4 wt %. The results (Δ*k* as a function of burnup) are shown in Figure 9, where it can be seen that both cases achieve a positive Δ*k* value. The Δ*k* for the case with 4.0 wt % ^{235}U enrichment becomes positive at a burnup of around 26 MWd/kgU, reaching a maximum of approximately 0.31% Δ*k* at around 40 MWd/kgU. The Δ*k* for the case with the 4.4 wt % ^{235}U enrichment becomes positive at a burnup of around 28 MWd/kgU, with a maximum of 0.29 % Δ*k* near 50 MWd/kgU.

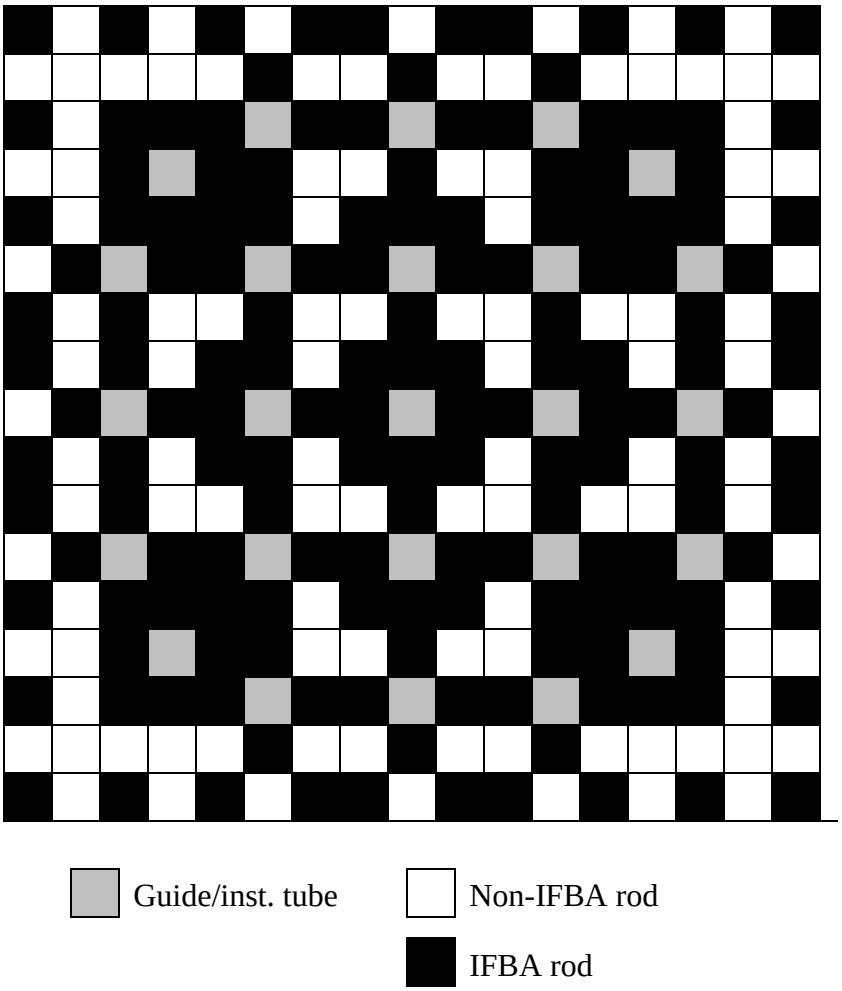

Figure 8 Fuel rod array (17 × 17) representing the 156 IFBA rod loading pattern

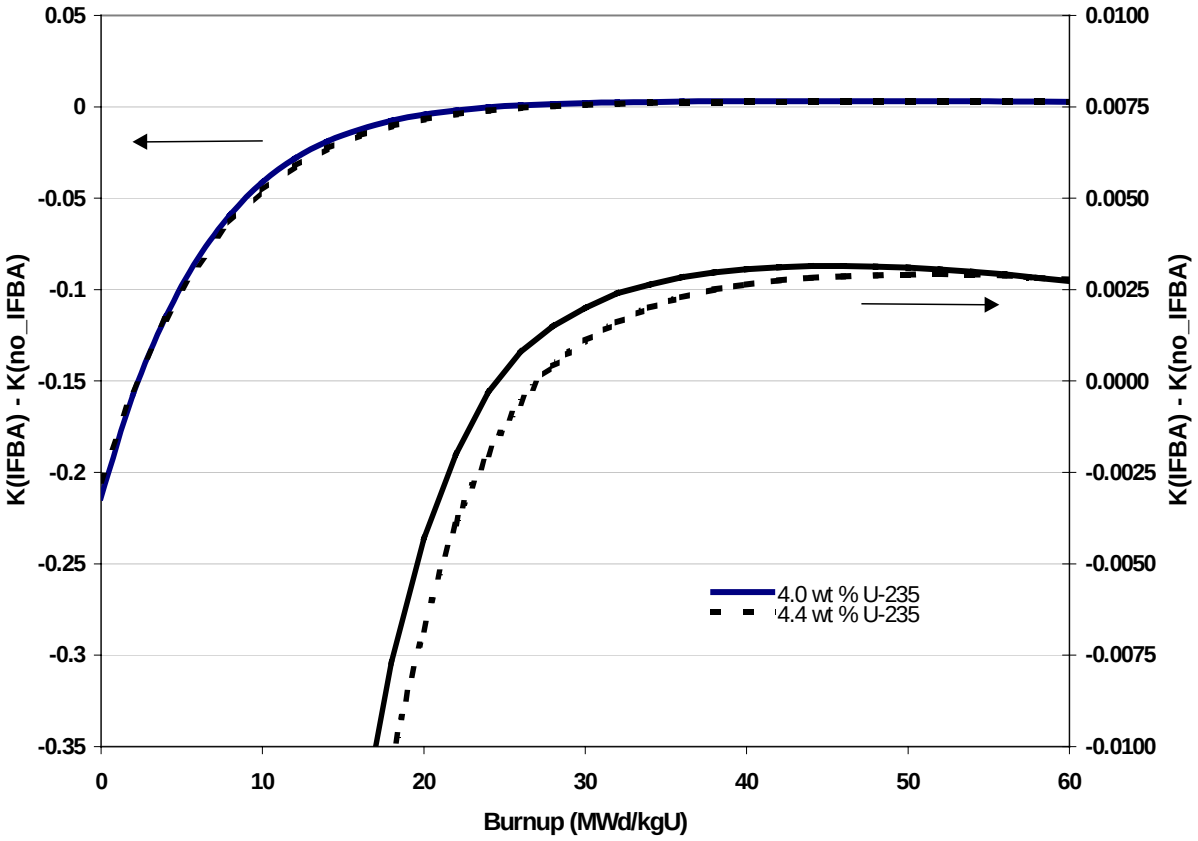

Figure 9 Comparison of Δ*k* values as a function of burnup between assemblies with and without IFBA rods (156 IFBA rods) for initial enrichments of 4.0 and 4.4 wt % ^{235}U. Note that the results are also plotted according to the enlarged scale on the right-hand side y-axis for clarity.

3.3.1.2 IFBA Analyses for 2.355 mg ^{10}B/inch

The three IFBA loading patterns considered in the previous subsection (80, 104 and 156 IFBA rods) were also studied with a poison loading of 2.355 mg ^{10}B/inch, for corresponding enrichments based on actual fuel data. The Δk values for the three various IFBA rod configurations are shown in Figure 10. These results demonstrate that for a given fuel enrichment, the positive reactivity effect increases with poison loading (i.e., number of IFBA rods).

An assembly design containing 104 IFBA rods was also evaluated with an enrichment of 4.25 wt % ^{235}U. The Δk values are shown in Figure 11, along with the reactivity differences from the previous calculation with 104 IFBA rods and 4.617 wt % ^{235}U enrichment.

Consistent with the results shown in the previous subsection, these results indicate that the k_{inf} values for fuel containing IFBA rods are not always less than the k_{inf} values for fuel without IFBA rods. The IFBA rods are shown to have a small, positive reactivity effect, as compared to assemblies without IFBA rods, at discharge burnups. For all of the IFBA cases considered, the maximum positive reactivity effect was determined to be 0.41%. However, it should be pointed out that this maximum value corresponds to the most heavily poisoned assembly design and, based on the available data, does not appear representative of typical IFBA assemblies.

For a fixed initial fuel enrichment, the positive reactivity effect has been shown to increase with increasing poison loading (i.e., both increasing ^{10}B loading and increasing number of IFBA rods).

Finally, from the results in this and previous subsection, it is clear that for a fixed poison loading the positive reactivity effect increases with decreasing fuel enrichment.

3.3.2 UO_2-Gd_2O_3 Integral Burnable Absorber Rods

A number of nuclear fuel vendors, including, CE, Framatome Cogema Fuels (formerly B&W), and Siemens, have manufactured a gadolinia-uranium (UO_2-Gd_2O_3) integral burnable absorber rod. These UO_2-Gd_2O_3 rods, or gadolinia rods, are fuel rods with Gd_2O_3 as an integral part of the fuel matrix. The weight percent or loading of Gd_2O_3 in each gadolinia-bearing rod and the number of gadolinia rods within an assembly are both variable. Further, the ^{235}U enrichment among the gadolinia-bearing and nongadolinia-bearing fuel rods is varied to a small extent in some designs (with the gadolinia bearing fuel rods having lower ^{235}U enrichment than the nongadolinia bearing fuel rods).

Various gadolinia loadings (wt % Gd_2O_3 and number of gadolinia-bearing rods) and enrichment combinations were studied in order to establish the reactivity effect as a function of burnup. The absorber loading and enrichment combinations considered are based on actual fuel assemblies, and were selected to encompass the range of known variations; including number of gadolinia rods, Gd_2O_3 wt %, and initial fuel enrichment.

Analyses are presented in the following subsections for two distinct fuel assembly designs that employ gadolinia-bearing rods: the CE 16×16 assembly design (which includes large water holes) and the Siemens 17×17 design. The Siemens assembly design does not include oversized water holes, and thus is expected to be representative of other similar fuel assembly designs (e.g., Framatome Cogema Fuels and Westinghouse designs that employ gadolinia-bearing rods).

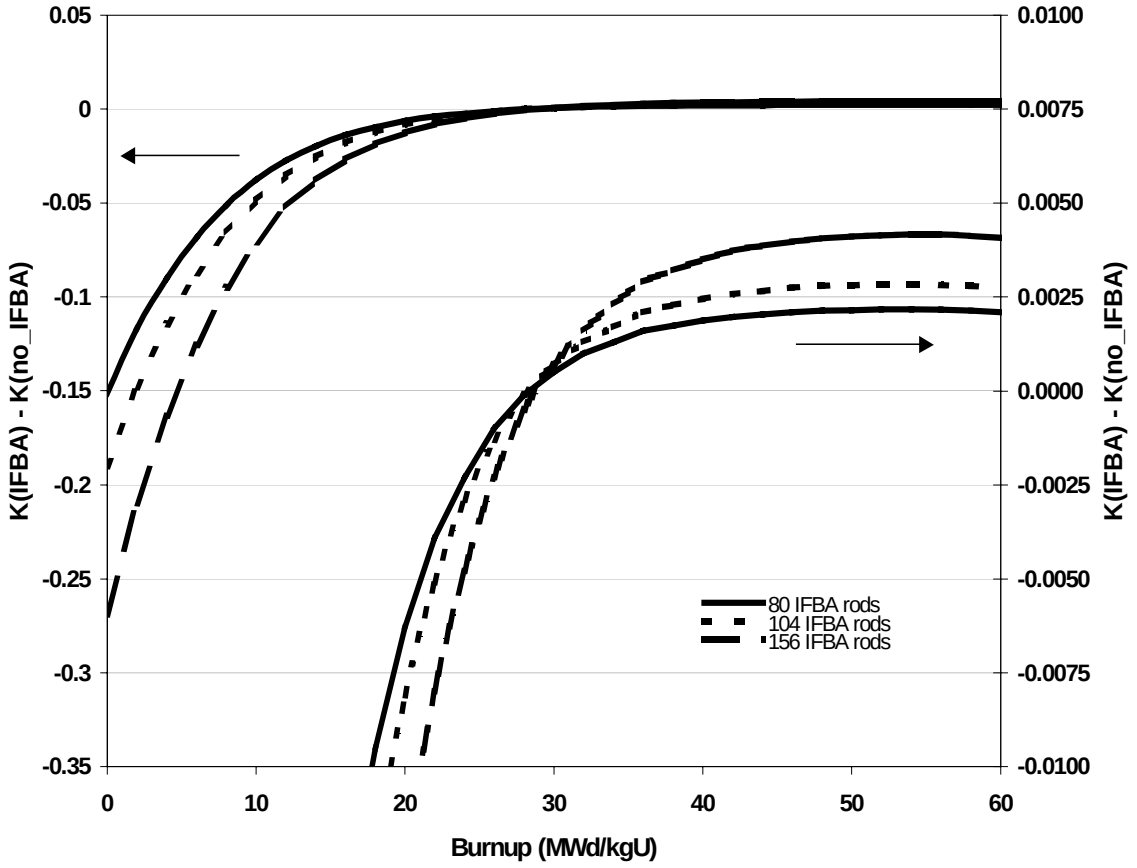

Figure 10 Comparison of Δk values as a function of burnup between assemblies with and without IFBA rods, with varied number of IFBA rods and an enrichment of 4.617 wt % ^{235}U. Note that the results are also plotted according to the enlarged scale on the right-hand side y-axis for clarity.

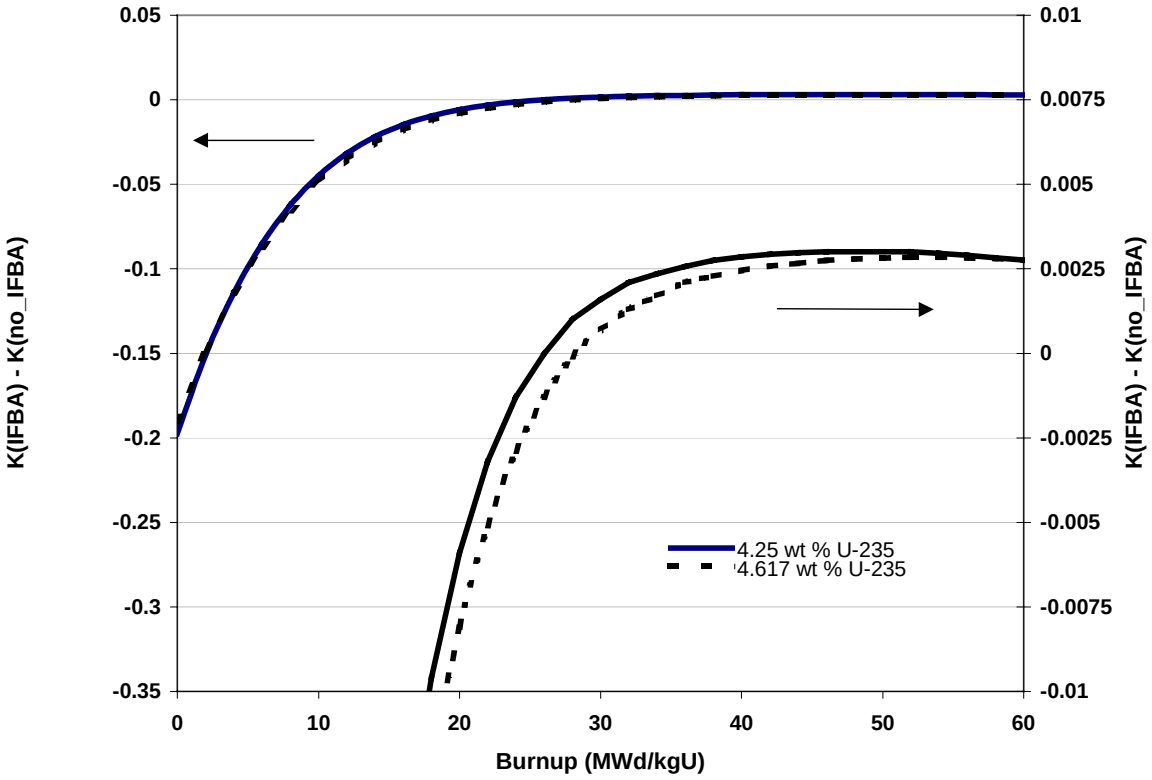

Figure 11 Comparison of Δk values as a function of burnup between assemblies with and without IFBA rods (104 IFBA rods) for initial enrichments of 4.25 and 4.617 wt % ^{235}U. Note that the results are also plotted according to the enlarged scale on the right-hand side y-axis for clarity.

3.3.2.1 Combustion Engineering (CE) Designs

The specifications for the CE gadolinia-bearing fuel assembly designs were obtained from Ref. 7. The actual fuel dimension specifications for these CE 16×16 assemblies are listed in Table 3. To facilitate the discussion, the fuel assembly designs are classified into two sets, based on their initial pin enrichments. The assembly designs within the two designated sets, D sets (D, D1 and D2) and E sets (E, E1 and E2), have variable numbers of gadolinia-bearing rods, as defined in Table 4. The corresponding fuel loading diagrams are illustrated in Figures 12 through 14. Figure 15 displays the D1 geometry as modeled in HELIOS.

Table 3 CE 16×16 fuel assembly specifications

Parameter	Dimensions (cm)
Rod pitch	1.285
Assembly pitch	20.78
Cladding outside diameter	0.97028
Cladding inside diameter	0.84328
Pellet outside diameter	0.82550
Water hole outside diameter	2.4892
Water hole Inside diameter	2.286
Array size	16×16
Number of water holes	5

Table 4 Fuel assembly data for the D and E sets of assembly designs

Fuel assembly	UO_2 fuel rod enrichment	No. of UO_2 fuel rods/assembly	No. of UO_2-Gd_2O_3 rods/assembly	Gd_2O_3/^{235}U wt % for UO_2-Gd_2O_3 rods
D	4.42/3.92	184/52	0	N/A
D1	4.42/3.92	176/52	8	6.00/4.42
D2	4.42/3.92	172/52	12	6.00/4.42
E	4.60/4.10	184/52	0	N/A
E1	4.60/4.10	176/52	8	8.00/4.60
E2	4.60/4.10	172/52	12	8.00/4.60

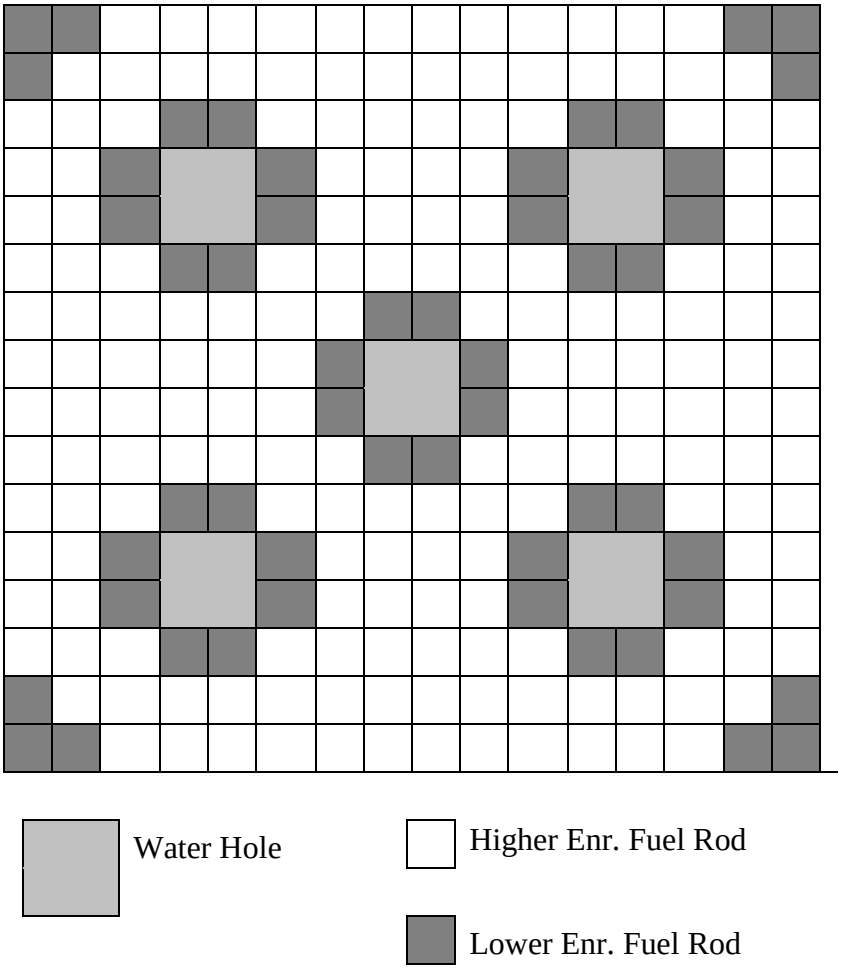

Figure 12 Fuel rod array (16 × 16) representing the D and E fuel assemblies loading pattern

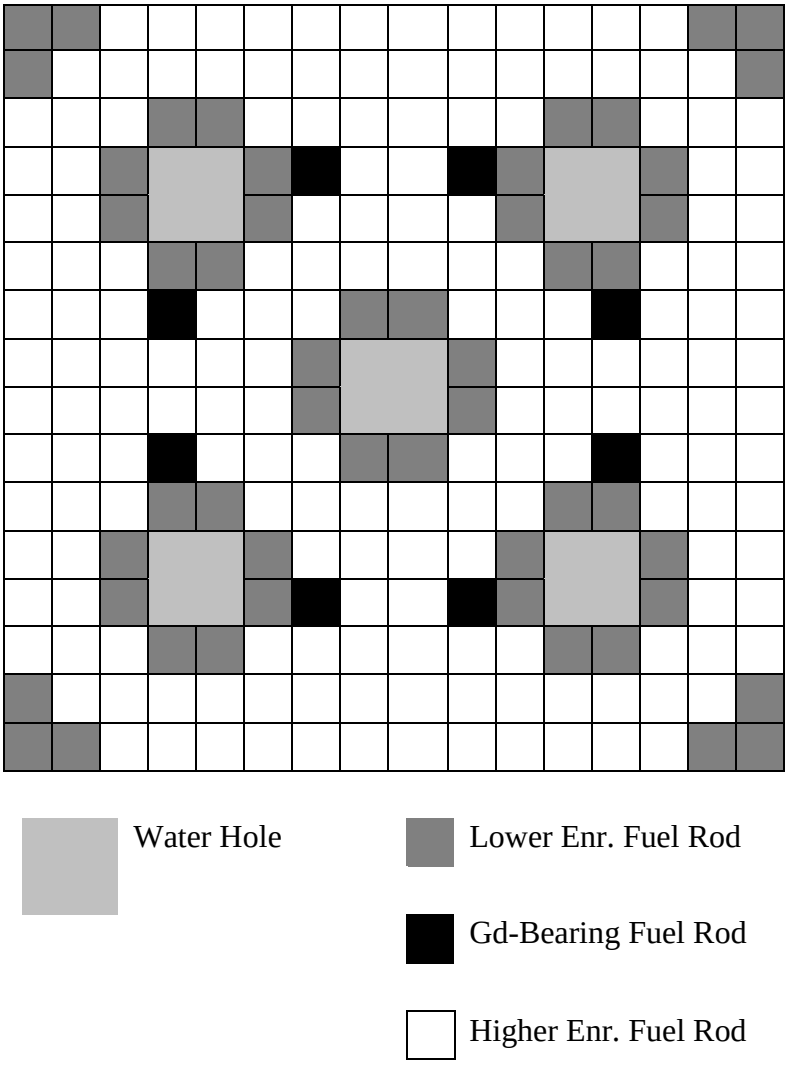

Figure 13 Fuel rod array (16 × 16) representing the D1 and E1 fuel assemblies loading pattern

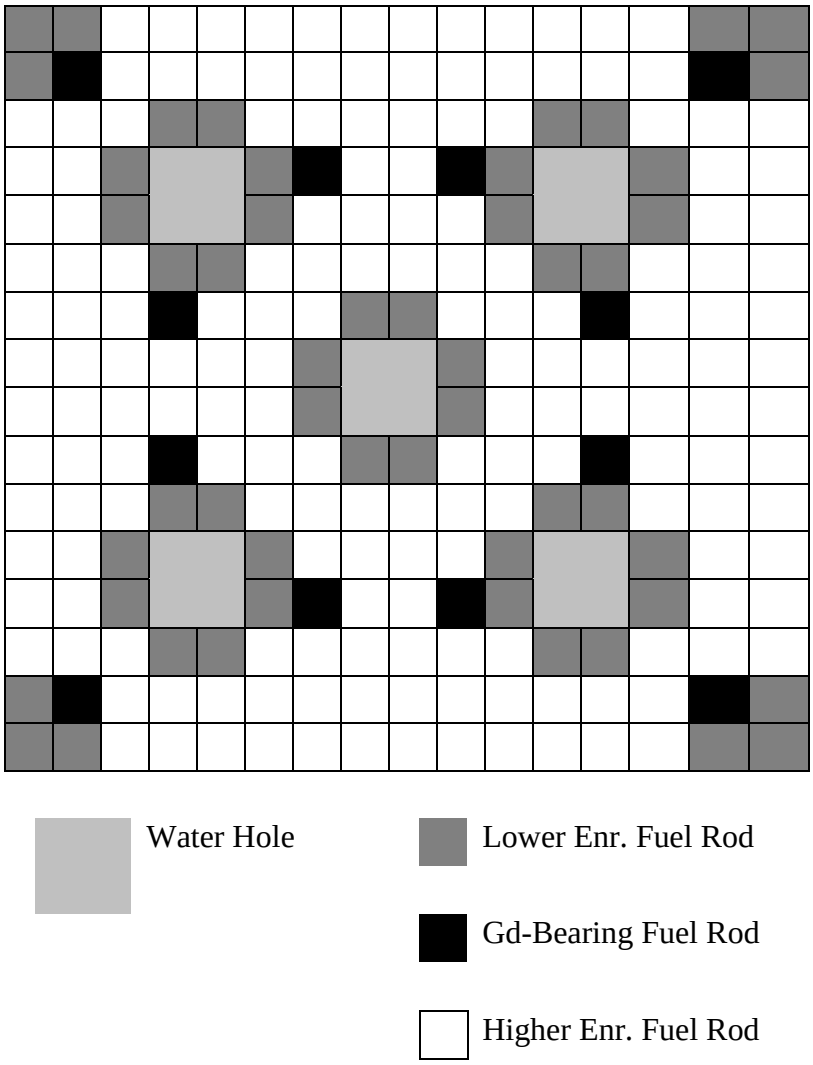

Figure 14 Fuel rod array (16 × 16) representing the D2 and E2 fuel assemblies loading pattern

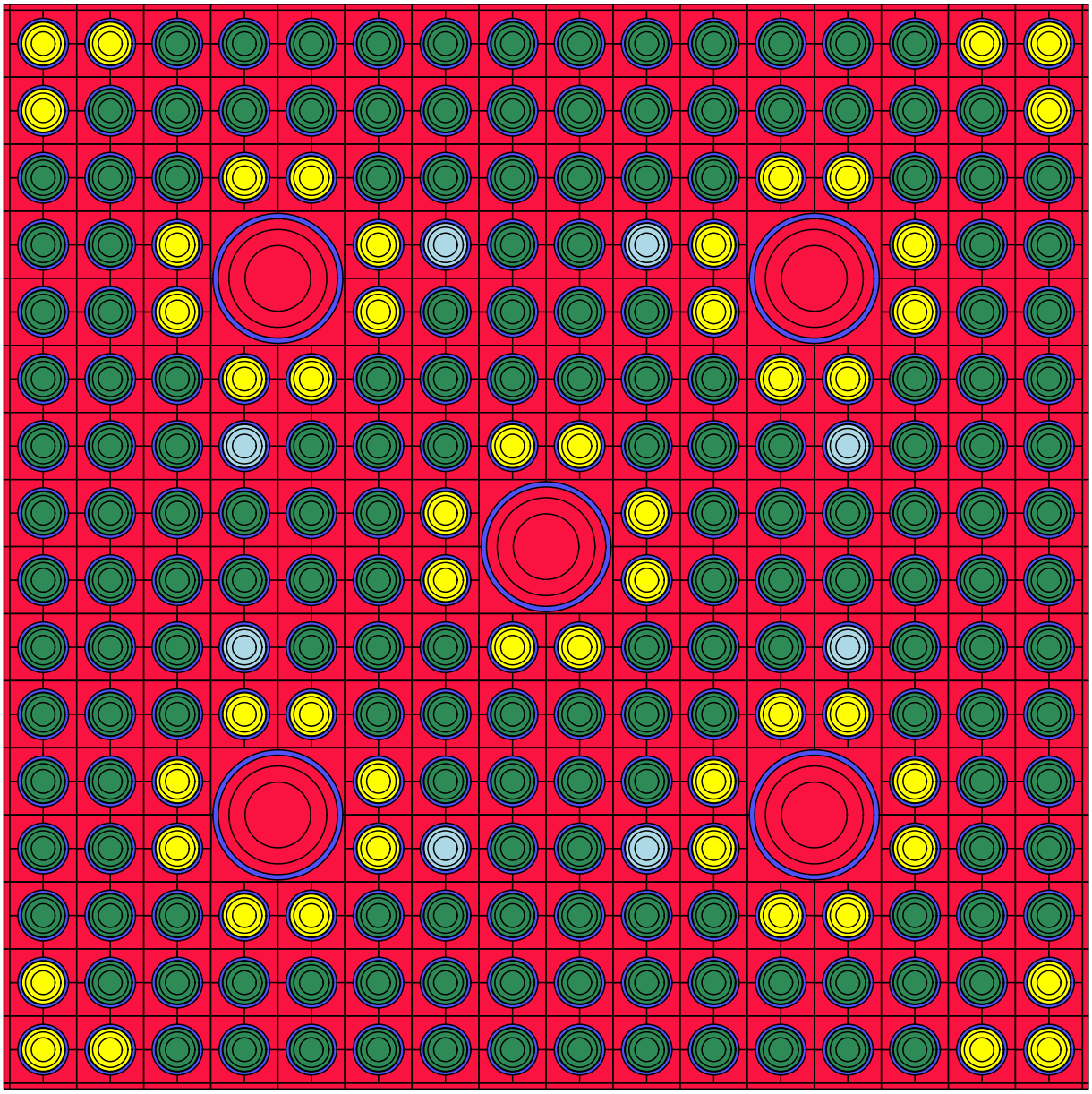

Figure 15 HELIOS calculational model of the D1 fuel assembly containing 8 UO_2-Gd_2O_3 rods

The effect of various numbers of gadolinia-bearing rods in the fuel assembly was studied. The D, D1, and D2 fuel assemblies were modeled according to Table 3 and Table 4, and the resulting Δk between the gadolinia-bearing (D1 and D2) and nongadolinia-bearing fuel (D) as a function of burnup is shown in Figure 16. It can be seen that the Δk never becomes positive for either of the gadolinia-bearing fuel assembly designs. In other words, the k_{inf} of the gadolinia-bearing fuel is always less than the k_{inf} of the nongadolinia fuel. Also note that the D2 fuel assembly, with 12 gadolinia-bearing rods, has a slightly more negative Δk than the D1 fuel assembly, which has only 8 gadolinia-bearing rods.

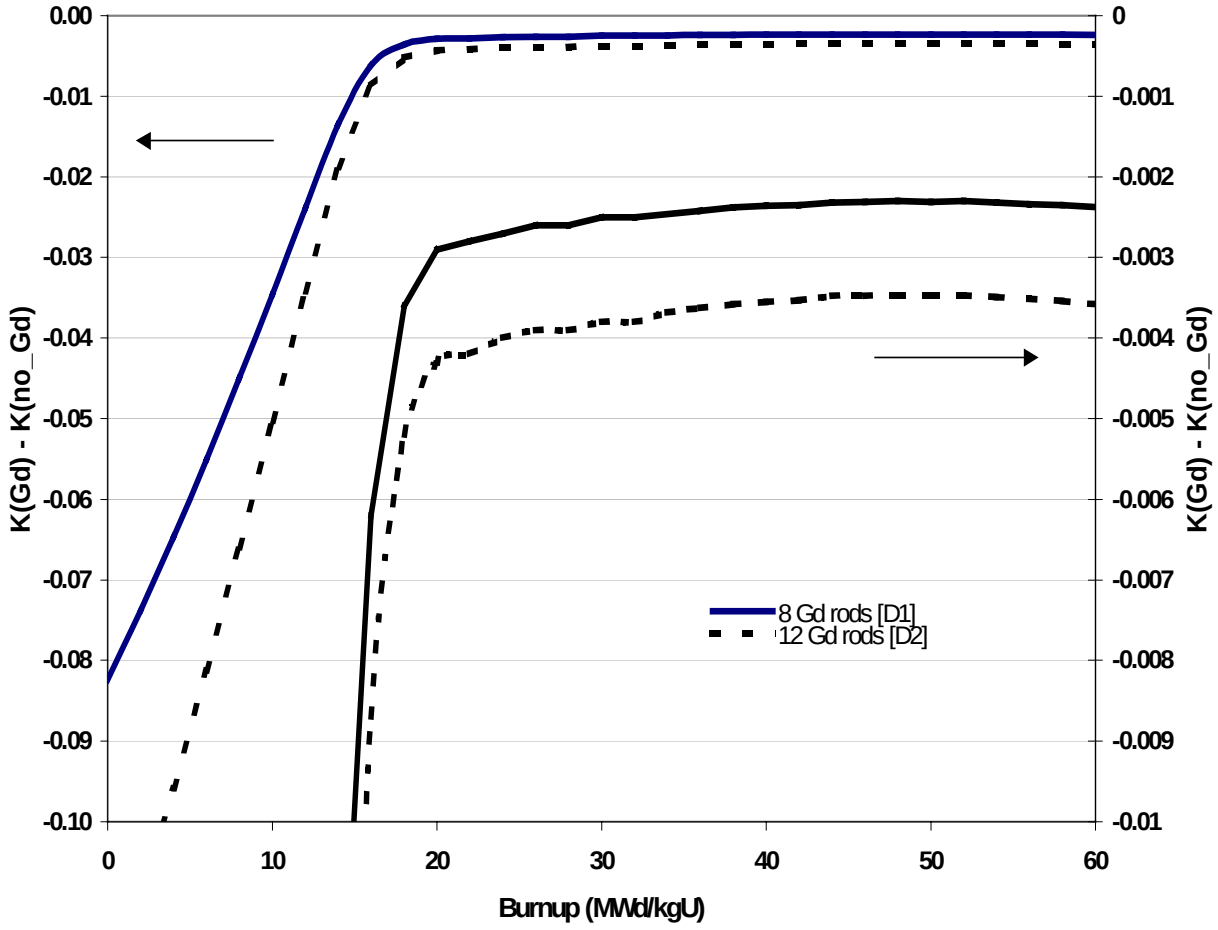

Figure 16 Comparison of Δk values as a function of burnup between the D assembly designs with gadolinia-bearing rods and the D assembly design (Figure 12) without gadolinia-bearing rods. Note that the results are also plotted according to the enlarged scale on the right-hand side y-axis for clarity.

The effect of various numbers of gadolinia-bearing rods was also studied for the E fuel assembly designs, modeled according to Tables 3 and 4. The resulting Δk as a function of burnup can be seen in Figure 17. Again, the Δk for both of the gadolinia-bearing fuel assembly types (E1 and E2) remains negative throughout the entire burnup cycle. Also note that Δk is slightly more negative for the higher ^{235}U enriched/higher gadolinia-loading E fuel assembly designs than for the lower ^{235}U enriched/lower gadolinia loading D fuel assembly designs.

The results from both the D and E fuel assembly designs indicate that the gadolinia-bearing fuel k_{inf} is less than the non-gadolinia-bearing fuel k_{inf} and the extent by which the reactivity of the gadolinia-bearing fuel assembly multiplication factor is reduced increases with increasing gadolinia loading (wt % Gd_2O_3 and the number of gadolinia-bearing rods).

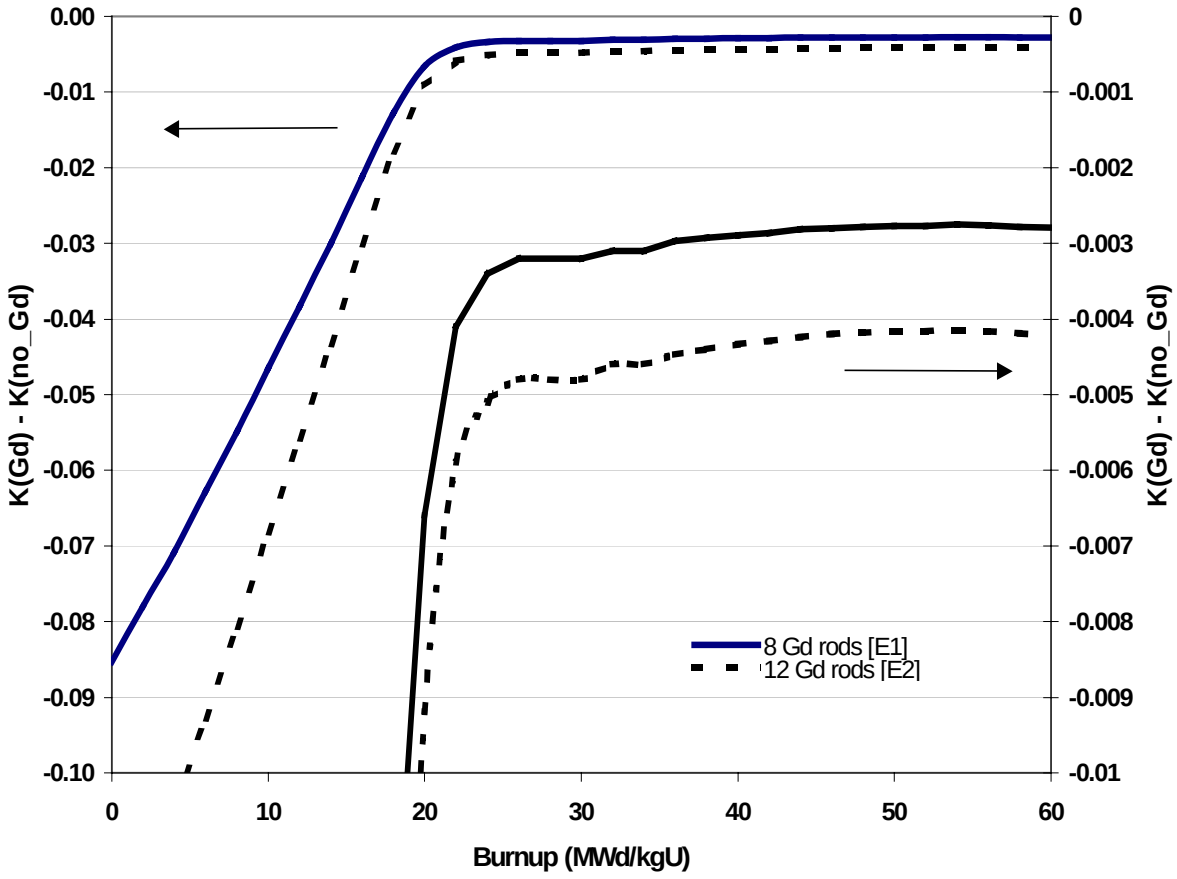

Figure 17 Comparison of Δk values as a function of burnup between the E assembly designs with gadolinia-bearing rods and the E assembly design (Figure 12) without gadolinia bearing rods. Note that the results are also plotted according to the enlarged scale on the right-hand side y-axis for clarity.

3.3.2.2 Siemens Designs

In addition to the CE assembly designs analyzed in the previous subsection, Siemens assembly designs with gadolinia-bearing rods have been analyzed. Four different 17×17-assembly designs with various integral burnable absorber rod loadings were considered. The common assembly specifications are listed in Table 5. All specifications for the Siemens gadolinia-bearing fuel assembly designs were obtained from Ref. 8. Figure 18 displays one of the fuel assemblies (M1) as modeled in HELIOS.

Table 5 Siemens 17×17 fuel assembly specifications

Parameter	Dimensions (cm)
Rod pitch	1.260
Assembly pitch	21.5
Cladding outside diameter	0.95504
Cladding inside diameter	0.83312
Pellet outside diameter	0.81661
Guide instrument tube outside diameter	1.2192
Guide instrument tube Inside diameter	1.1379
Array size	17×17
Number of fuel rods	264
Number of guide instrument tubes	25

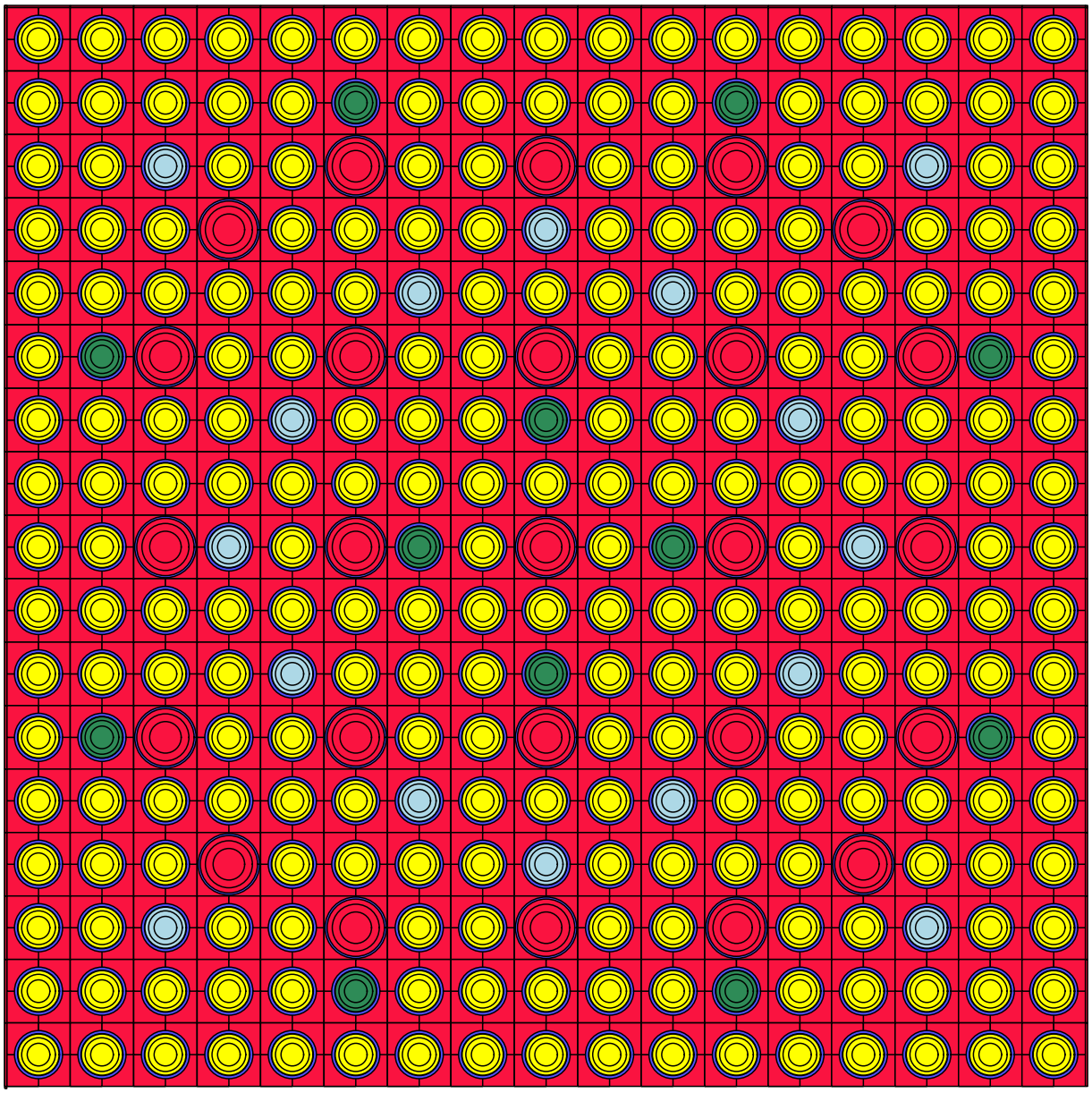

Figure 18 HELIOS calculational model of M1 fuel assembly

The assembly designs considered, designated M1–M4, are illustrated in Figures 19–22 and summarized in Table 6. Unpoisoned, equivalent enrichment reference cases (corresponding to M1–M4, respectively) were also analyzed and used for comparison.

Table 6 Fuel assembly data for the M1–M4 assembly designs

Fuel assembly	UO_2 fuel rod enrichment	No. of UO_2 fuel rods/assembly	No. of UO_2- Gd_2O_3 rods/assembly	Gd_2O_3 /^{235}U wt %for UO_2- Gd_2O_3 rods
M1	4.25	236	16 12	8.00/3.91 4.00/4.08
M2	4.25	240	16 8	8.00/3.91 4.00/4.08
M3	4.25	244	16 4	6.00/3.99 2.00/4.16
M4	4.25	260	4	2.00/4.16

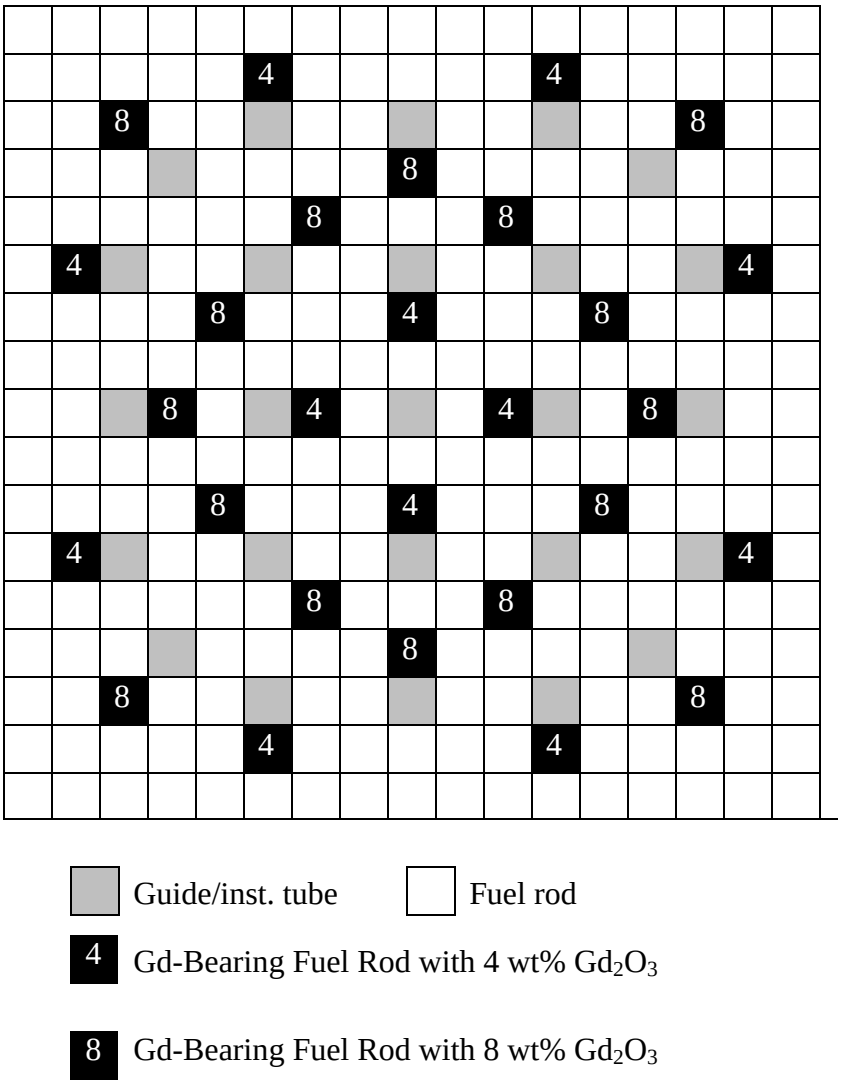

Figure 19 Fuel rod array (17 × 17) representing the M1 loading pattern

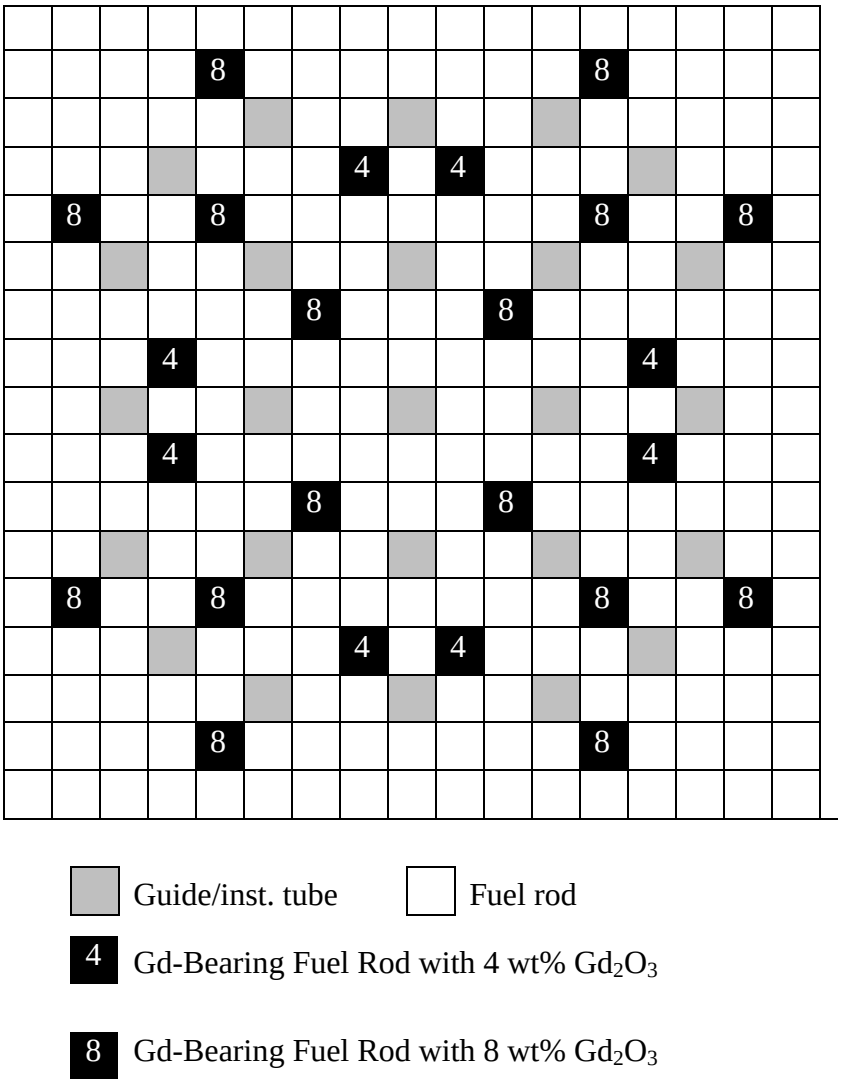

Figure 20 Fuel rod array (17 × 17) representing the M2 loading pattern

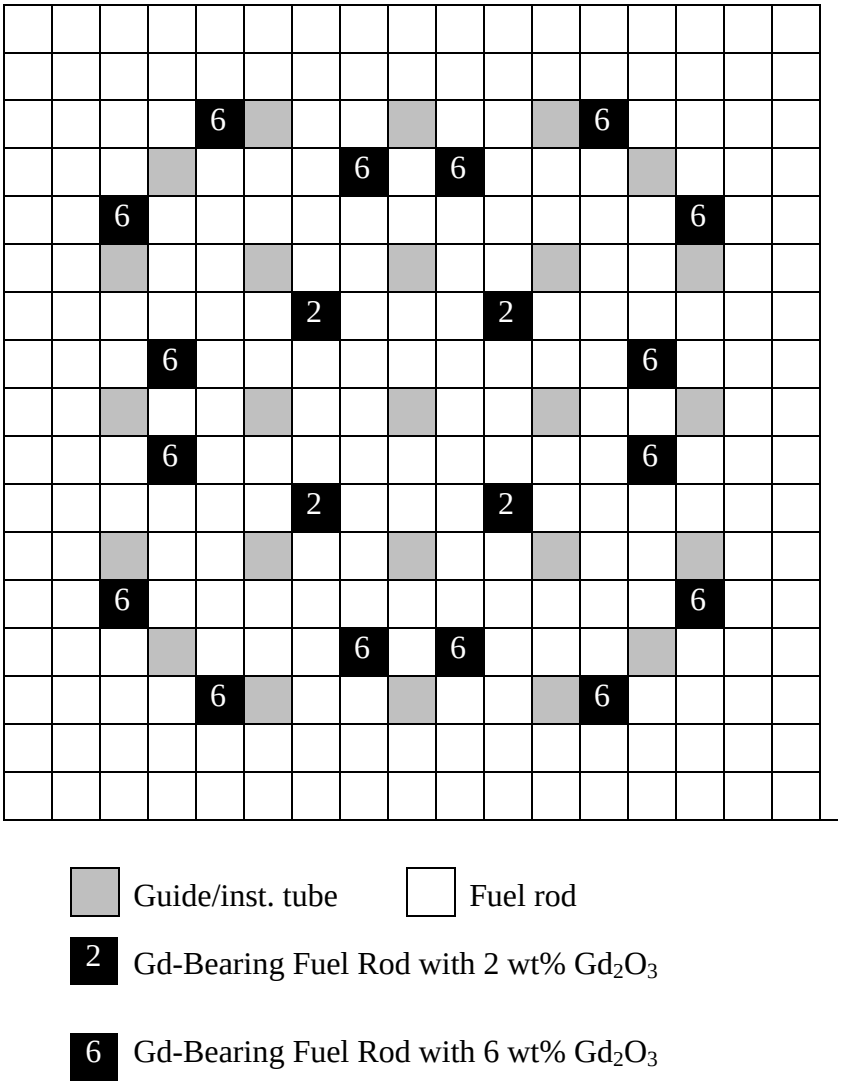

Figure 21 Fuel rod array (17 × 17) representing the M3 loading pattern

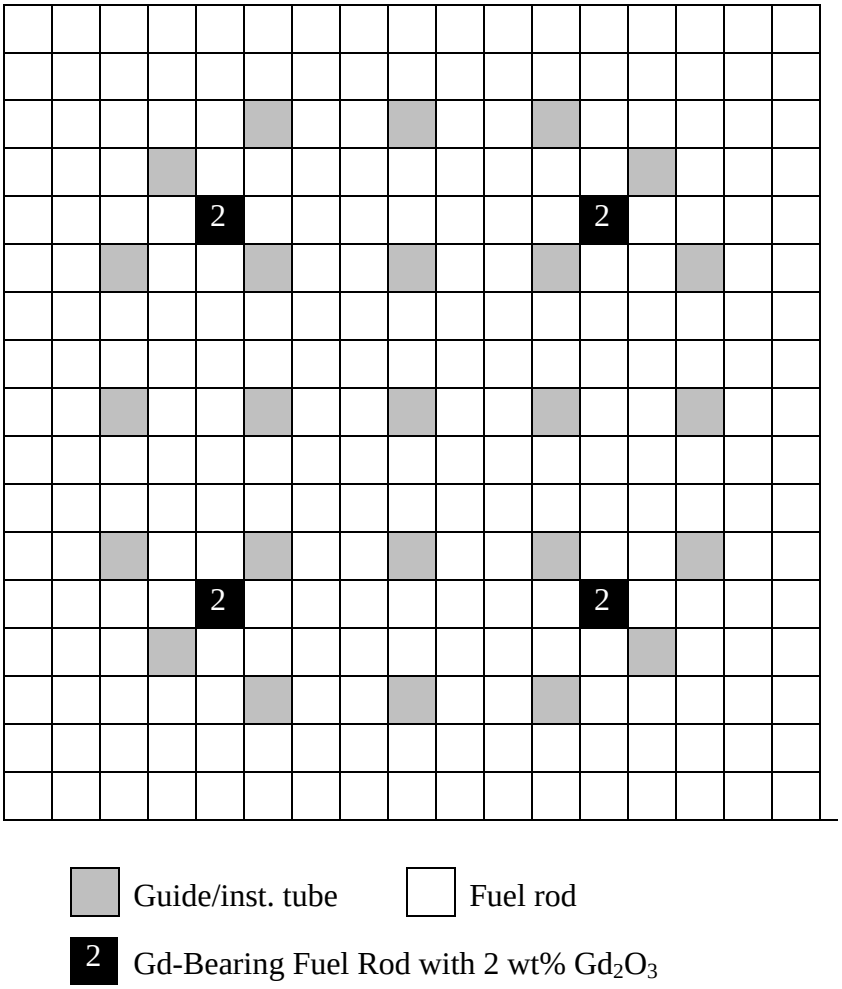

Figure 22 Fuel rod array (17 × 17) representing the M4 loading pattern

The k_{inf} values as a function of burnup for the unpoisoned reference case (corresponding to M1) and the poisoned M1 case are compared in Figure 23. The Δk as a function of burnup for the assemblies are shown in Figures 24 and 25, where it can be seen that all of the gadolinia-bearing fuel assembly designs yield a negative Δk. As mentioned earlier, each case (M1–M4) has a separate reference case that does not contain any gadolinia.

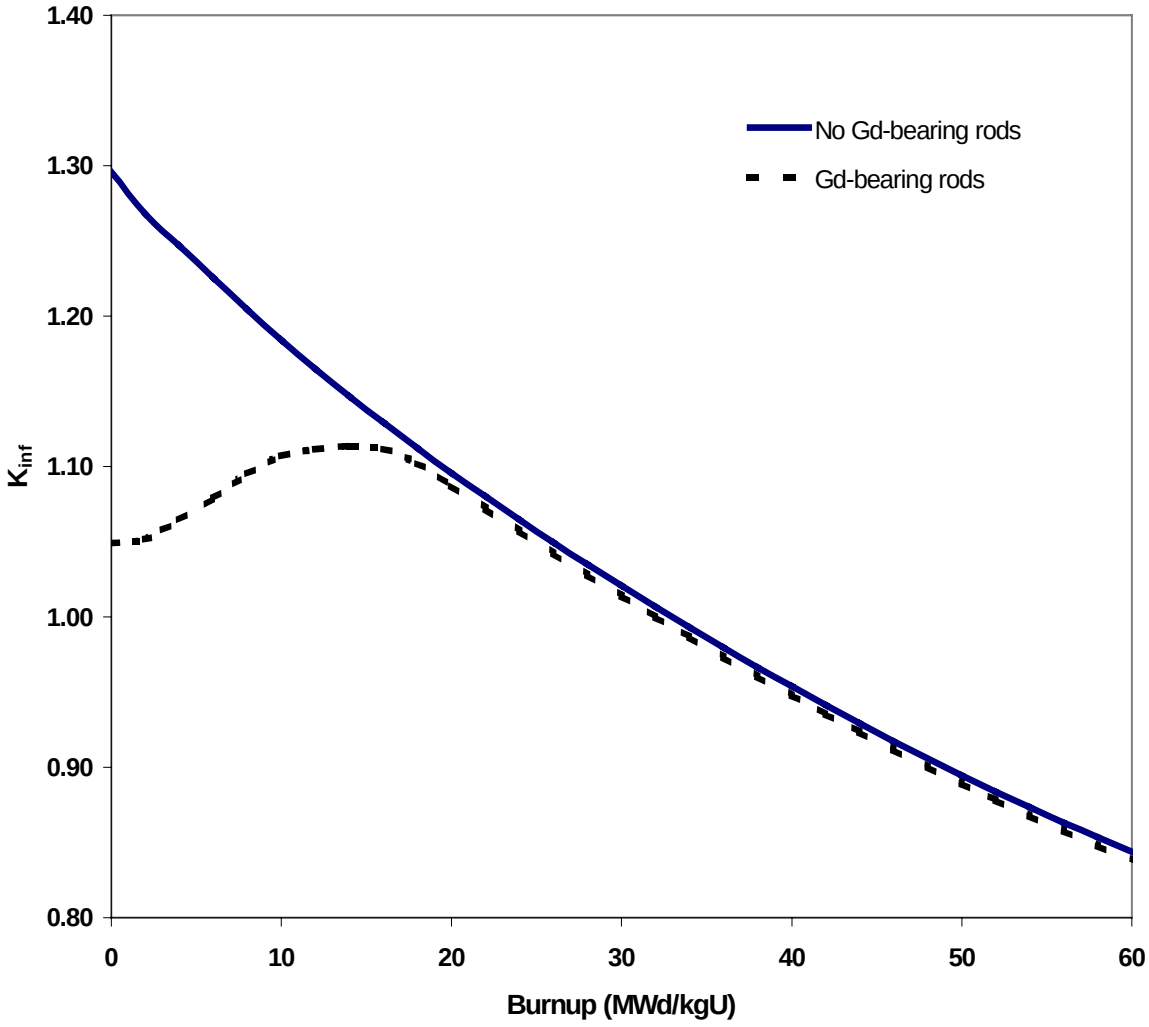

Figure 23 Comparison of k_{inf} values with and without gadolinia-bearing rods present (M1 assembly)

Consistent with the results shown in the previous subsection, these results confirm that the k_{inf} values for fuel assemblies with gadolinia-bearing rods are always less than the k_{inf} values for fuel assemblies without gadolinia-bearing rods. Further, the amount by which the k_{inf} values are lower increases with increasing gadolinia loading.

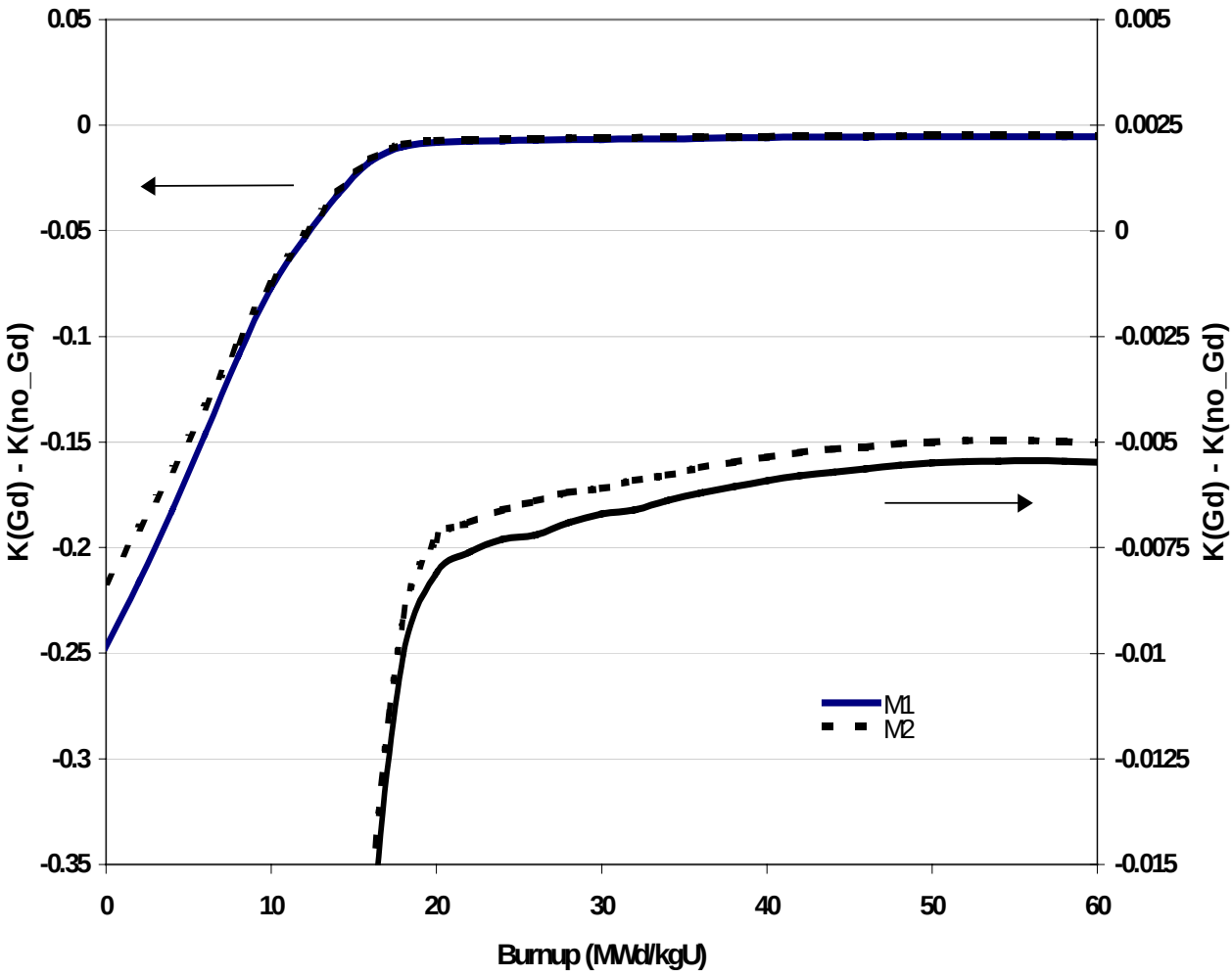

Figure 24 Comparison of Δk values as a function of burnup between assemblies with (M1 and M2) and without gadolinia-bearing integral burnable absorber rods. Note that the results are also plotted according to the enlarged scale on the right-hand side y-axis for clarity.

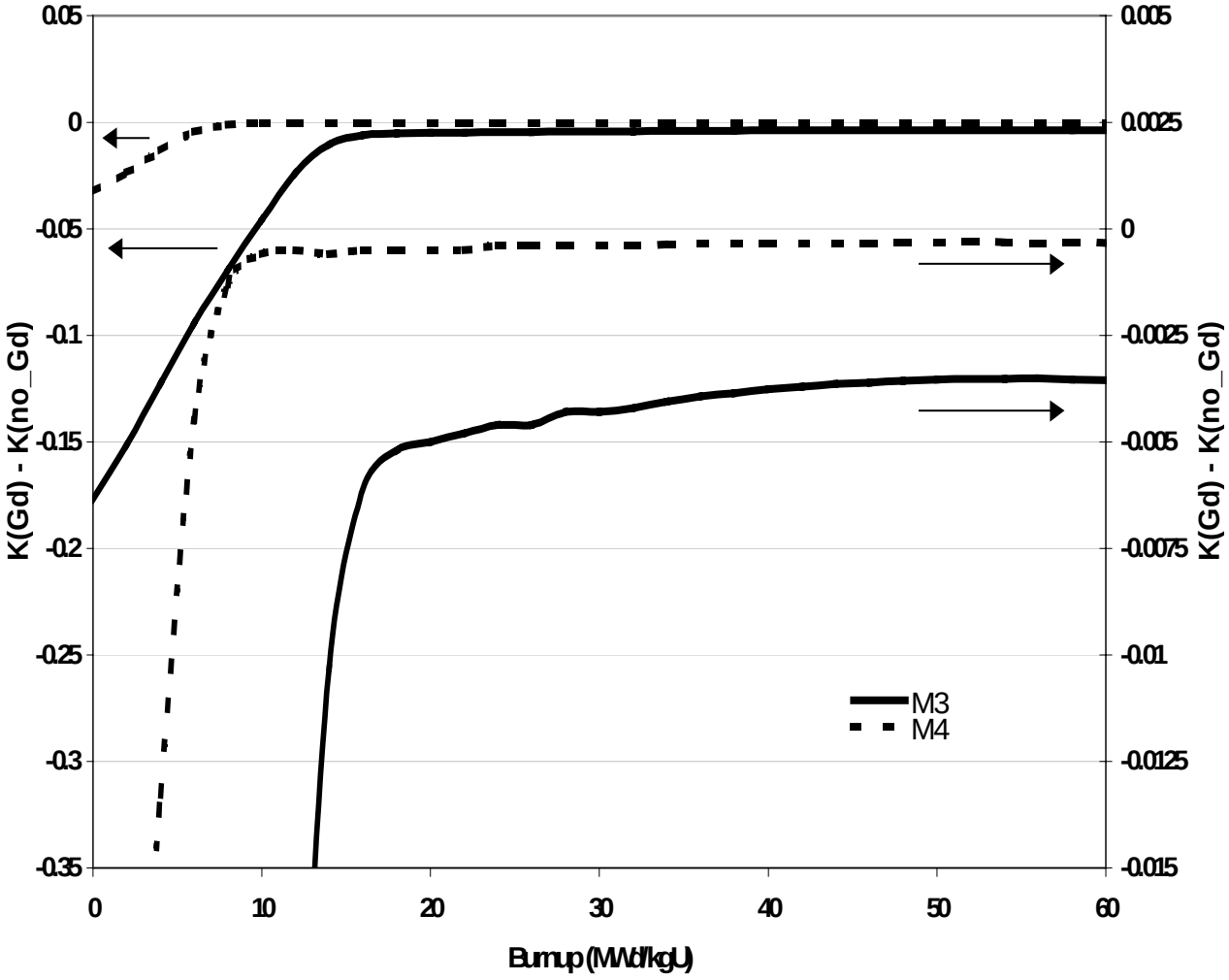

Figure 25 Comparison of Δk values as a function of burnup between assemblies with (M3 and M4) and without gadolinia-bearing integral burnable absorber rods. Note that the results are also plotted according to the enlarged scale on the right-hand side y-axis for clarity.

3.3.3 UO_2-Er_2O_3 Integral Burnable Absorber Rods

In addition to UO_2-Gd_2O_3 rods, CE has manufactured an integral burnable absorber containing erbia (Er_2O_3). Assemblies with erbia-bearing rods are far less prevalent than assemblies with gadolinia-bearing rods. Similar to the UO_2-Gd_2O_3 rods, the erbia-bearing rods include the burnable absorber (Er_2O_3) as an integral part of the fuel matrix. The weight percent of the erbia and the number of erbia-bearing rods within an assembly are both variable, as well as the ^{235}U enrichment.

Common specifications[9] for the CE 14×14 erbia-bearing fuel assembly designs are listed in Table 7. Figure 26 shows the geometry of one of the considered fuel assemblies (containing 60 erbia rods). The two unique erbia-bearing fuel assembly lattices considered are shown in Figures 27 and 28. The enrichment of the fuel pins is 4.3 wt % ^{235}U and the weight percent of Er_2O_3 is 2.0. Consistent with previous calculations, the fuel enrichment is maintained for the integral burnable absorber rods.

Calculations were performed for (1) the actual assembly specifications (as shown in Figures 27 and 28) and (2) an artificial reference condition in which the erbia was removed from the erbia-bearing fuel rods. The k_{inf} values as a function of burnup for the two conditions are compared in Figure 29. The results (Δk values) from the calculations, where the number of erbia-bearing fuel rods were varied, are shown in Figure 30. It can be seen that the k_{inf} value for the non-erbia-bearing fuel assembly remains higher than the k_{inf} values corresponding to the erbia-bearing fuel assemblies (i.e., the Δk values are always negative). Further, the difference between the k_{inf} value for erbia-bearing fuel and that for the non-erbia-bearing fuel increases with increasing erbia loading.

Table 7 CE 14×14 fuel assembly specifications (Er_2O_3)

Parameter	Dimensions (cm)
Rod pitch	1.47
Assembly pitch	20.8
Cladding outside diameter	1.1176
Cladding inside diameter	0.97536
Pellet outside diameter	0.95631
Water hole outside diameter	2.4079
Water hole inside diameter	2.3063
Array size	14×14
Number of fuel rods	176
Number of water holes	5

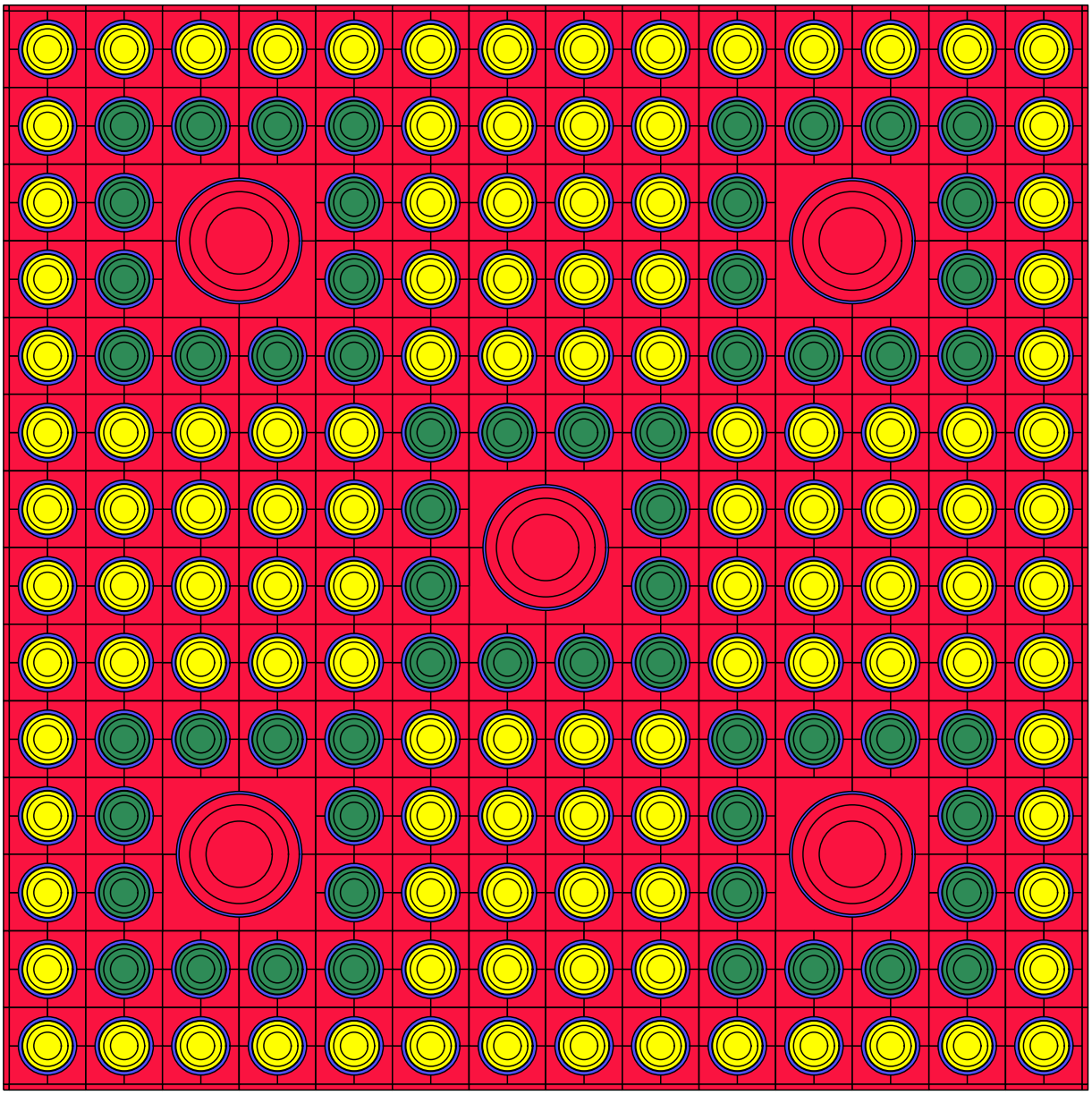

Figure 26 HELIOS calculational model of a fuel assembly containing 60 erbia-bearing fuel rods

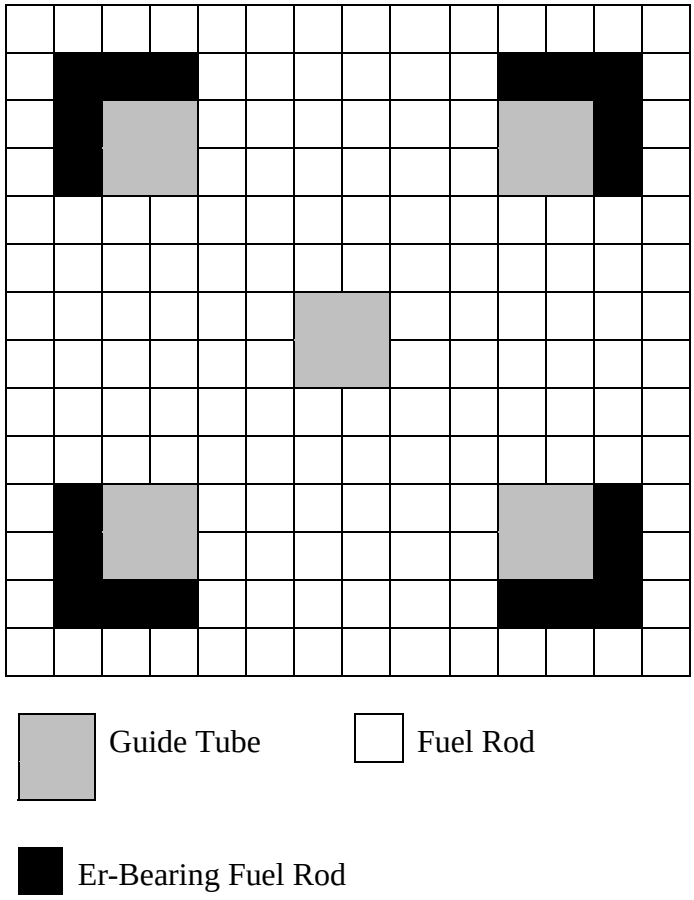

Figure 27 Fuel rod array (14 × 14) representing the 20 UO_2-Er_2O_3 rod loading pattern

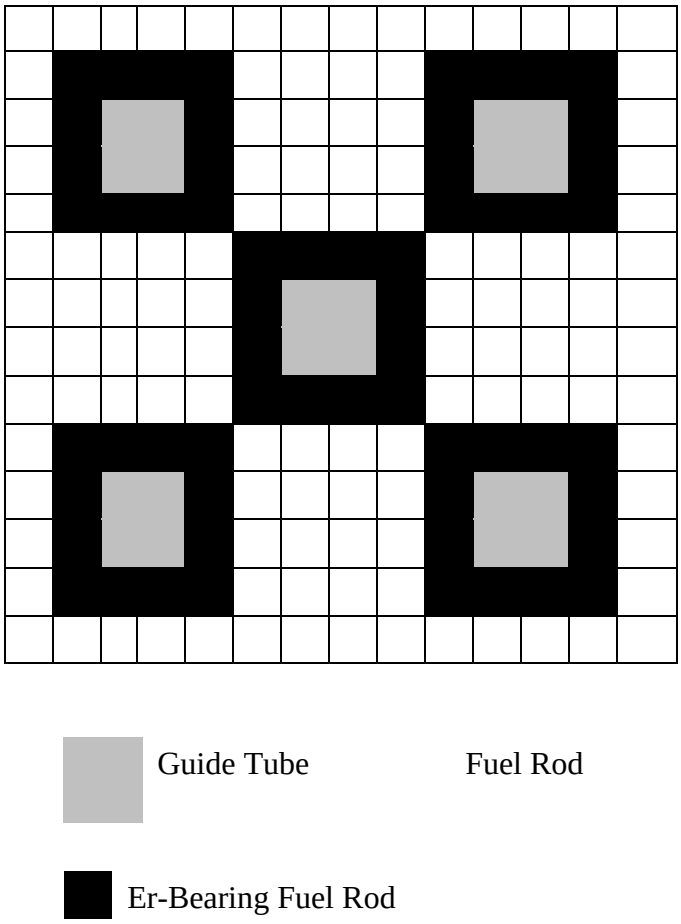

Figure 28 Fuel rod array (14 × 14) representing the 60 UO_2-Er_2O_3 rod loading pattern

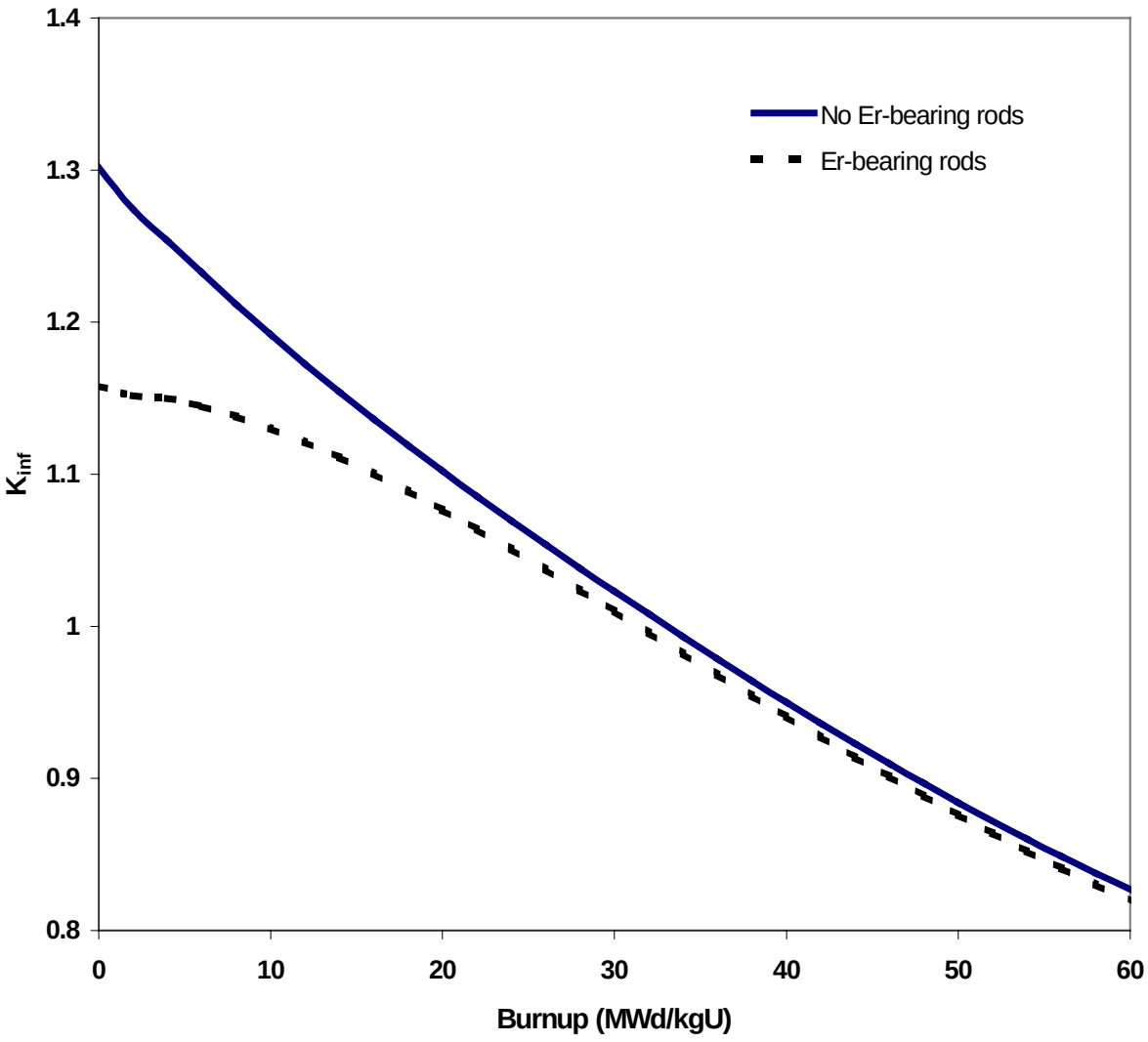

Figure 29 Comparison of k_{inf} values with Er_2O_3 integral burnable absorber rods present (assembly with 60 Er_2O_3 integral burnable absorber rods) and without Er_2O_3 integral burnable absorber rods present

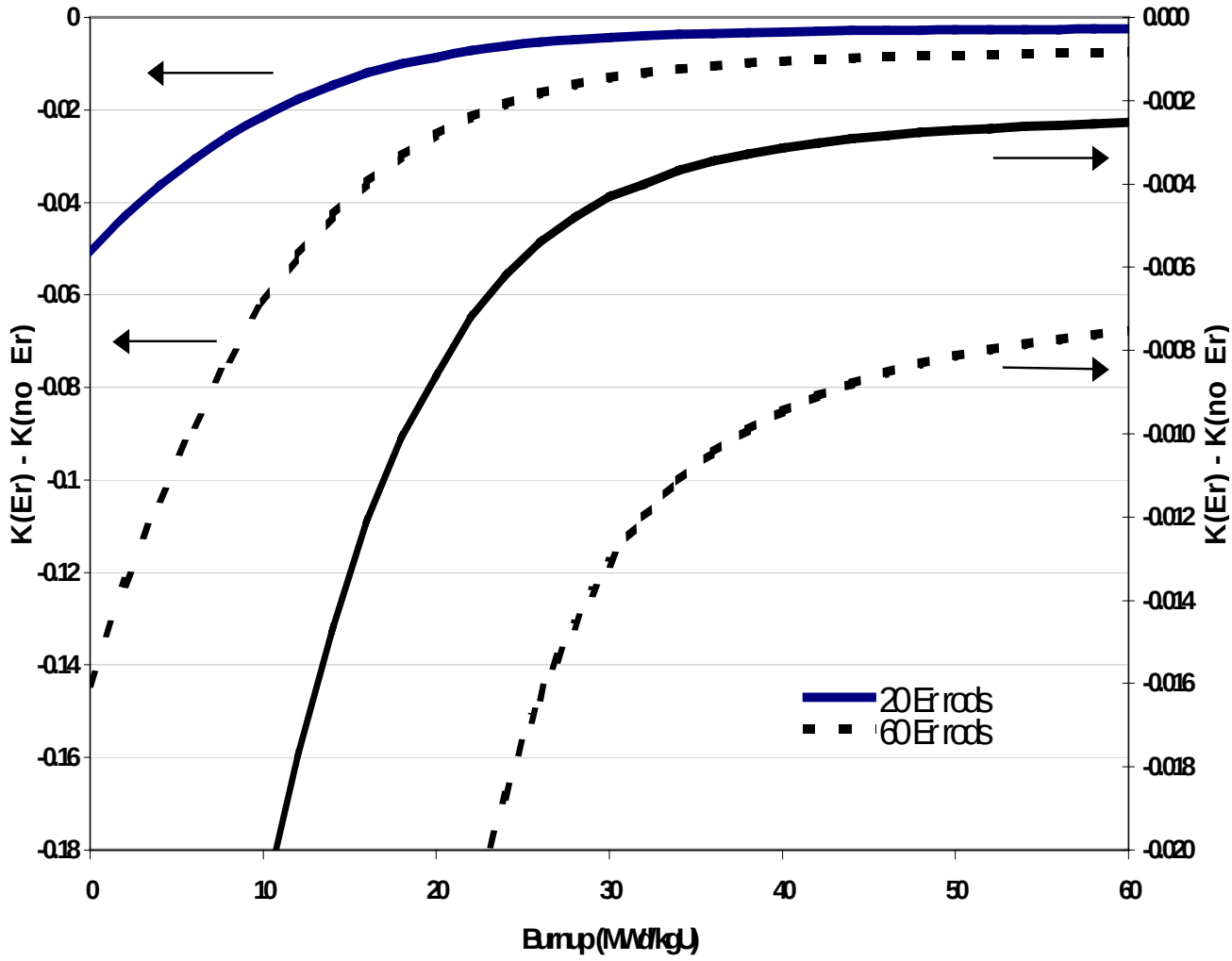

Figure 30 Comparison of Δk values as a function of burnup between assemblies with and without Er_2O_3 fuel rods present. The fuel rods have a ^{235}U enrichment of 4.3 wt % and the Er_2O_3 integral burnable absorber rods contain 2.0 wt % erbia. Note that the results are also plotted according to the enlarged scale on the right-hand side y-axis for clarity.

3.3.4 Al_2O_3-B_4C Integral Burnable Absorber Rods

Another integral burnable absorber manufactured by CE consists of solid rods containing aluminum pellets with uniformly dispersed boron carbide particles (Al_2O_3-B_4C), clad in Zircaloy. Unlike the IFBA, UO_2-Gd_2O_3, and UO_2-Er_2O_3, these rods do not contain fuel. However, the B_4C rods are an *integral*, nonremovable part of the fuel assembly. The weight percent of B_4C and the number of rods per assembly are variable.

The limited specifications for actual CE fuel assembly designs with Al_2O_3-B_4C rods were obtained from Ref. 99. Figure 31 dispays the geometry of one of the CE fuel assembly designs considered containing 12 Al_2O_3-B_4C rods. The actual fuel dimension specifications for these CE 14×14 assemblies are listed in Table 8 and the assembly lattices are shown in Figures 32–34.

The unpoisoned reference case also consists of a square 14×14 fuel rod array, although, without any Al_2O_3-B_4C integral burnable absorber rods (the Al_2O_3-B_4C rods have been replaced with fuel pins). The Al_2O_3-B_4C rods have an initial enrichment of 4.0 wt % B_4C, and the fuel rods have an initial enrichment of 4.0 wt % ^{235}U. The k_{inf} values as a function of burnup with and without Al_2O_3-B_4C rods present are compared in Figure 35. The results (Δk as a function of burnup) are shown in Figure 36, where it can be seen that the case maintains a negative Δk throughout the entire burnup cycle.

Table 8 CE 14×14 fuel assembly specifications (Al_2O_3-B_4C)

Parameter	Dimensions (cm)
Rod pitch	1.47
Assembly pitch	20.8
Cladding outside diameter	1.1176
Cladding inside diameter	0.97536
Pellet outside diameter	0.91948
Water hole outside diameter	2.4079
Water hole inside diameter	2.3063
Array size	14×14
Number of fuel rods	176
Number of water holes	5

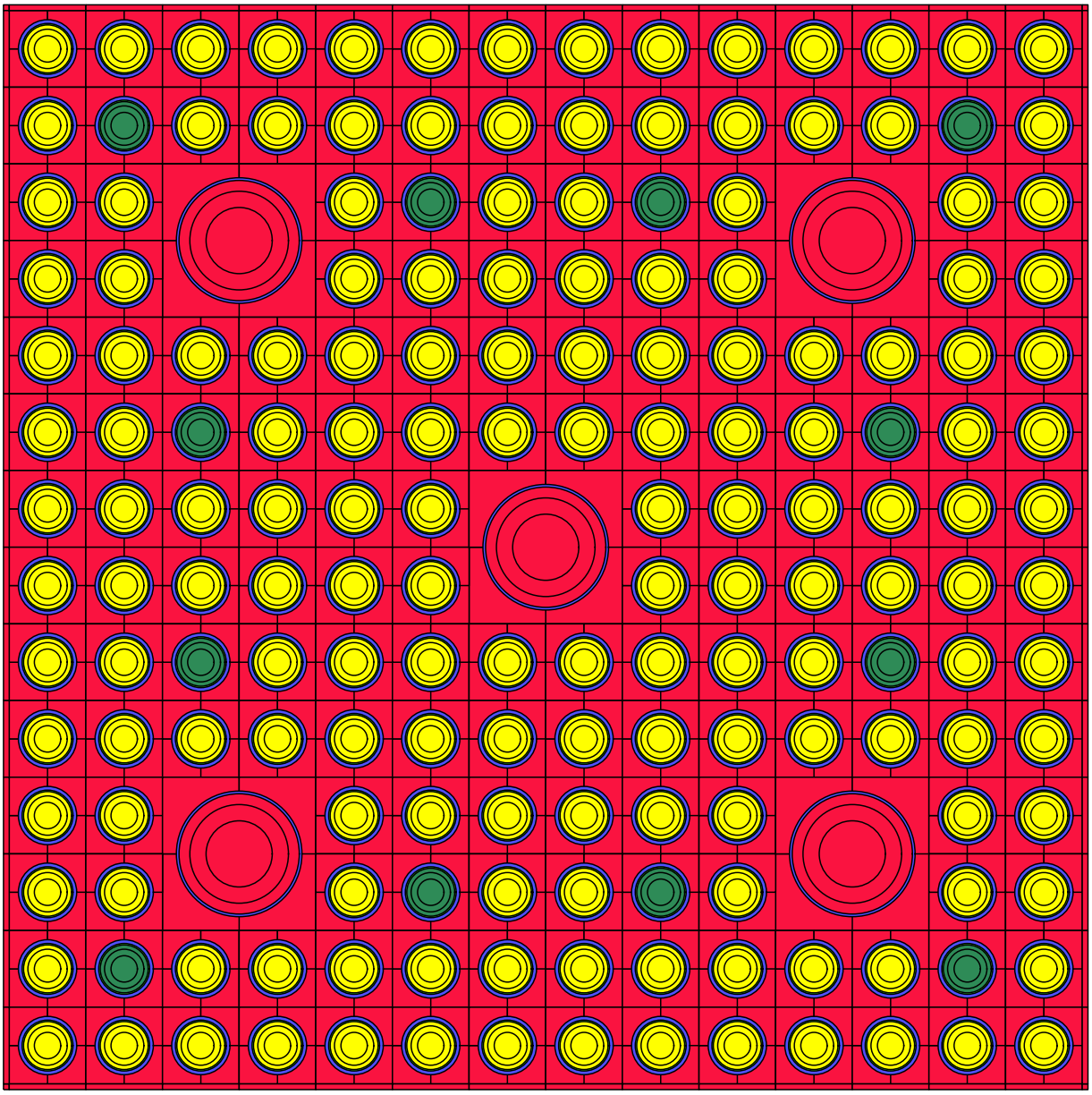

Figure 31 HELIOS calculational model of a fuel assembly containing 12 Al_2O_3-B_4C rods

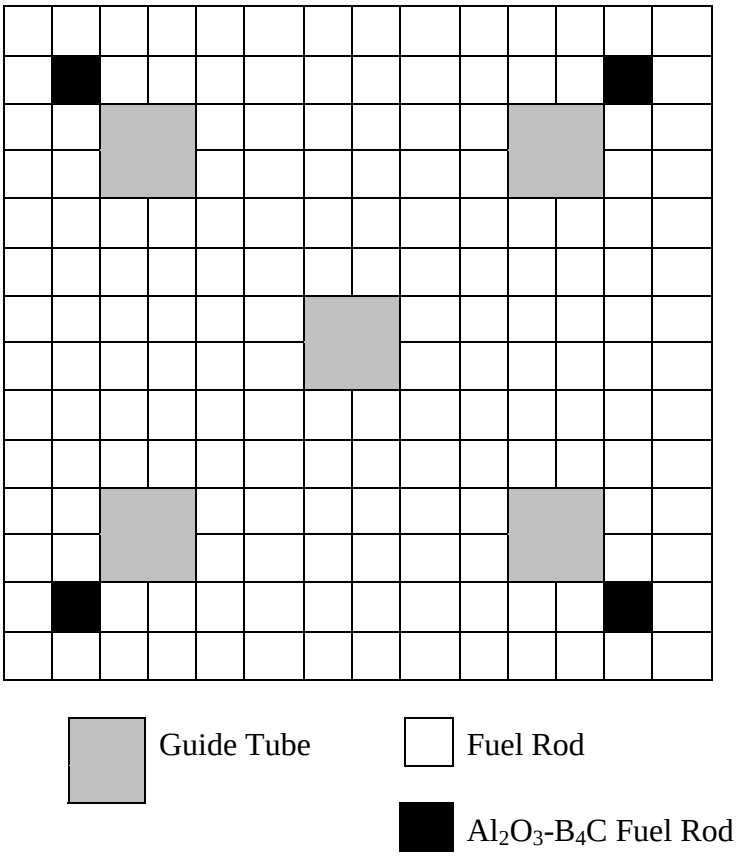

Figure 32 Fuel rod array (14 × 14) representing the 4 Al_2O_3-B_4C rod loading pattern

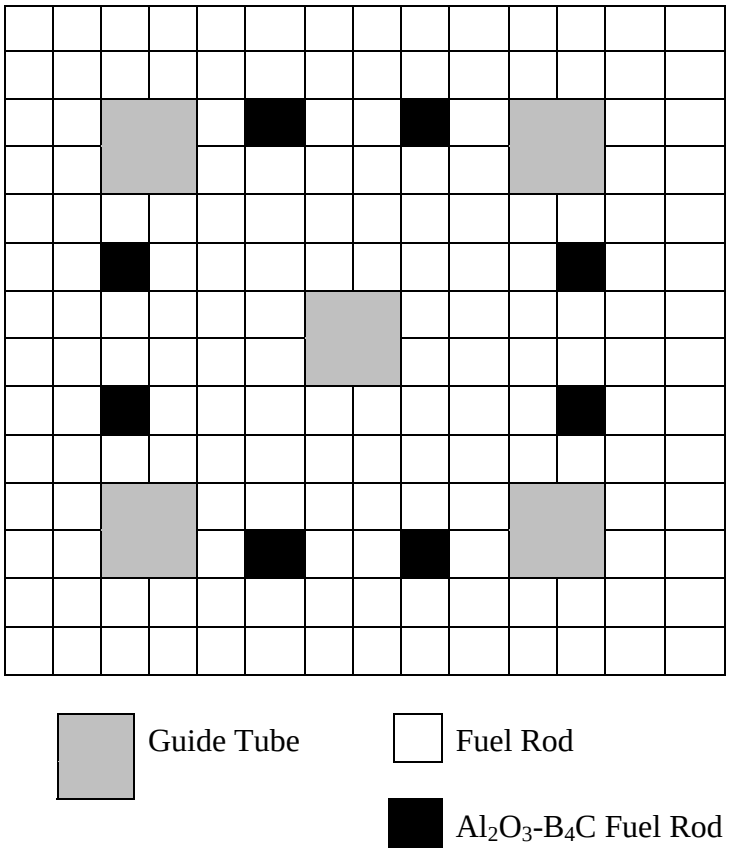

Figure 33 Fuel rod array (14 × 14) representing the 8 Al_2O_3-B_4C rod loading pattern

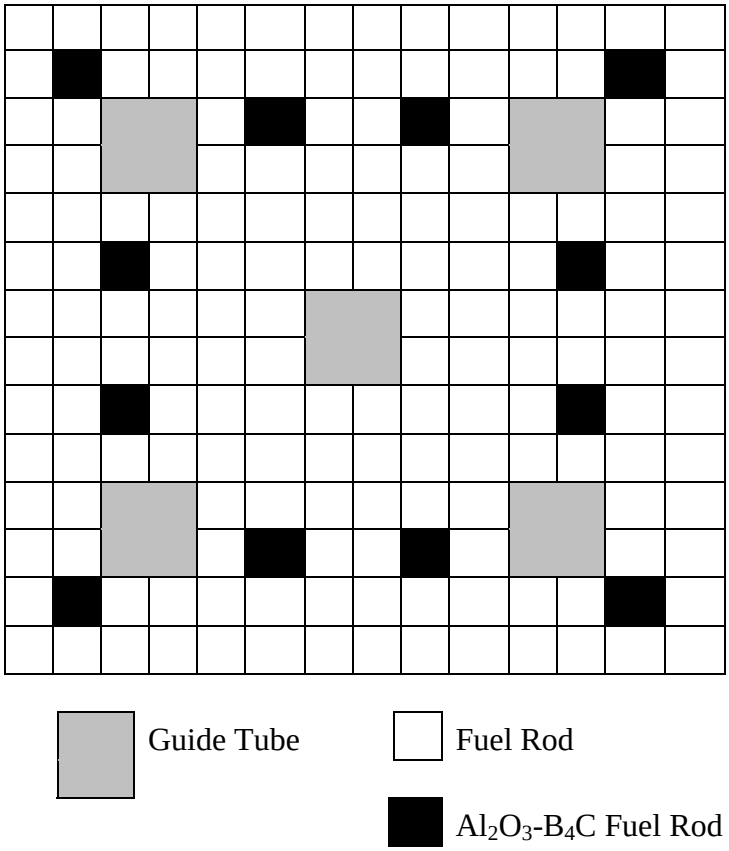

Figure 34 Fuel rod array (14 × 14) representing the 12 Al_2O_3-B_4C rod loading pattern

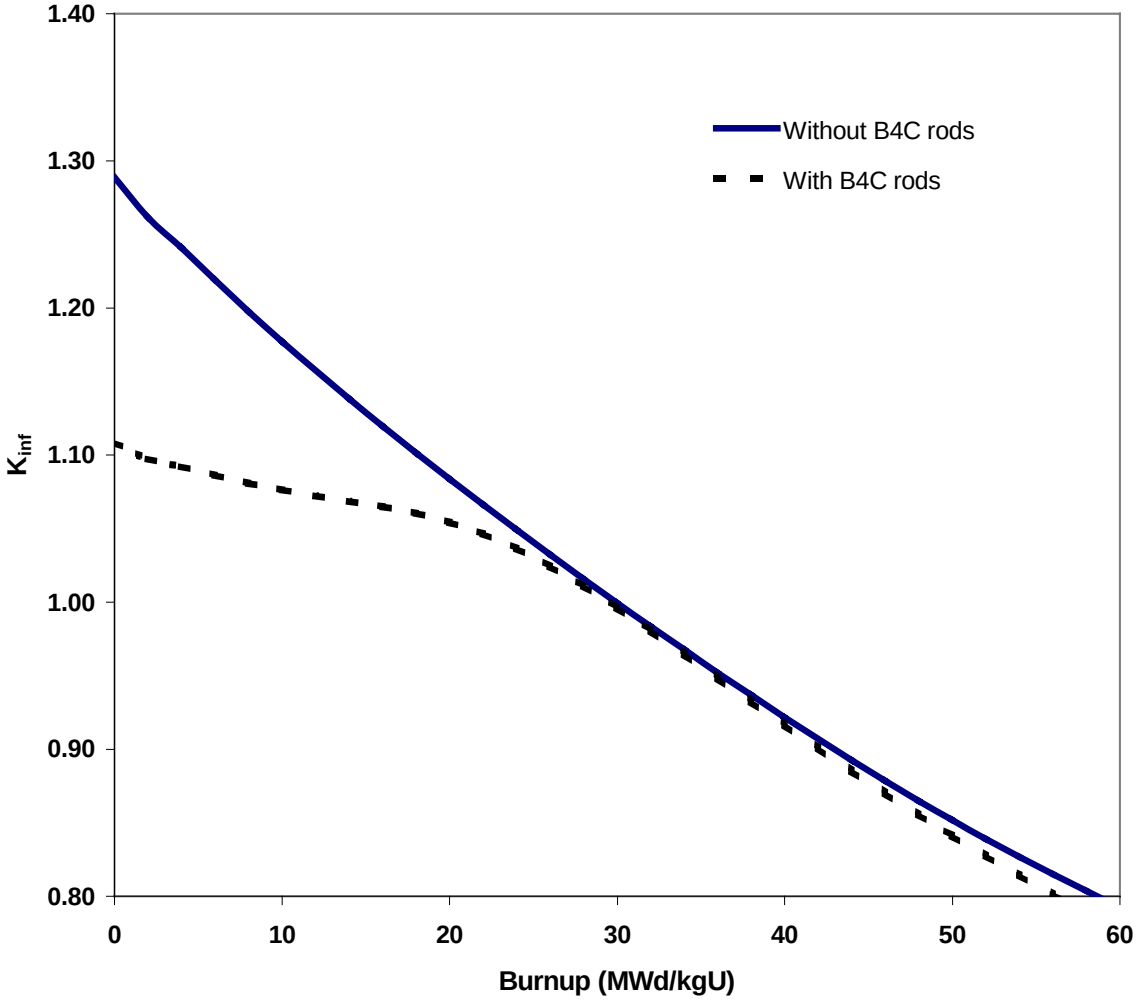

Figure 35 Comparison of k_{inf} values with (12 B_4C rods) and without B_4C integral burnable absorber rods present

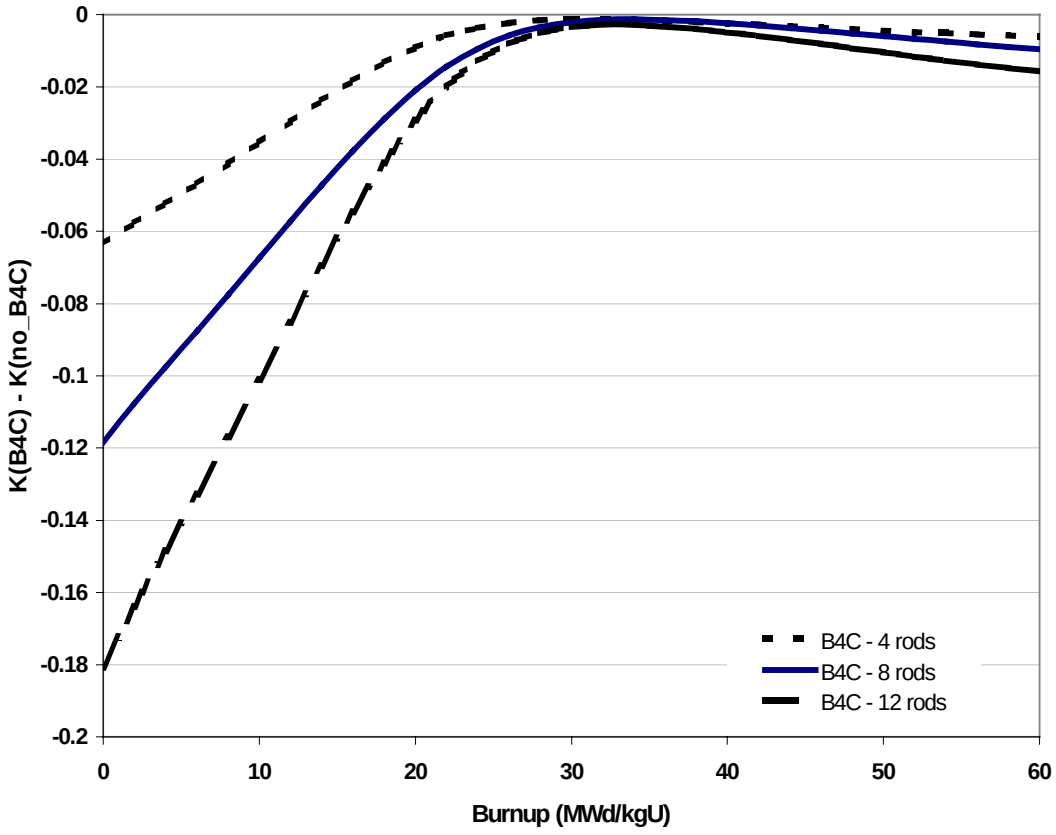

Figure 36 Comparison of Δk values as a function of burnup between assemblies with and without Al_2O_3-B_4C rods present. The fuel rods have a ^{235}U enrichment of 4 wt % and the Al_2O_3-B_4C integral burnable absorber rods have 4 wt % B_4C.

3.3.5 Additional Integral Burnable Absorber Rod Studies

All of the analyses presented in the previous sections are for actual fuel assembly designs obtained from plant data. In an attempt to better understand the impact of integral burnable absorber rods for variations outside of those shown in the previous sections, additional studies are presented in this section. These studies are intended to clarify trends and/or relationships between the various characteristics that are variable (e.g., poison loading and initial fuel enrichment). Note that although these studies are based on actual fuel assembly designs, the parameters are artificially varied outside of the known range. Consequently, the results in this section should be used to enhance understanding, and not for quantifying the reactivity effects.

3.3.5.1 Variations of Gadolinia Loading and Initial Fuel Enrichment

This additional study involves variations in poison loading and fuel enrichment in a CE fuel assembly design with Gd_2O_3 integral burnable absorber rods. The base case consists of a square 16×16 fuel rod array with no burnable absorber rods present as shown in Figure 12. The dimensions and specification of the fuel assembly are provided in Tables 3 and 4. For the remaining cases with integral burnable absorber rods present, the assembly layout is shown in Figure 13.

Calculations with varying weight percent gadolinia in the integral burnable absorber rods (UO_2-Gd_2O_3) have been performed in order to investigate the sensitivity to gadolinia enrichments. Gadolinia enrichments of 4, 6, and 8 wt % were considered, while the ^{235}U enrichment was fixed at 3.78/3.28. The Δk values for the various gadolinia enrichment cases as function of burnup are shown in Figure 37. Consistent with earlier results for actual fuel assembly designs, these results show that the negative Δk increases with increasing gadolinia loading.

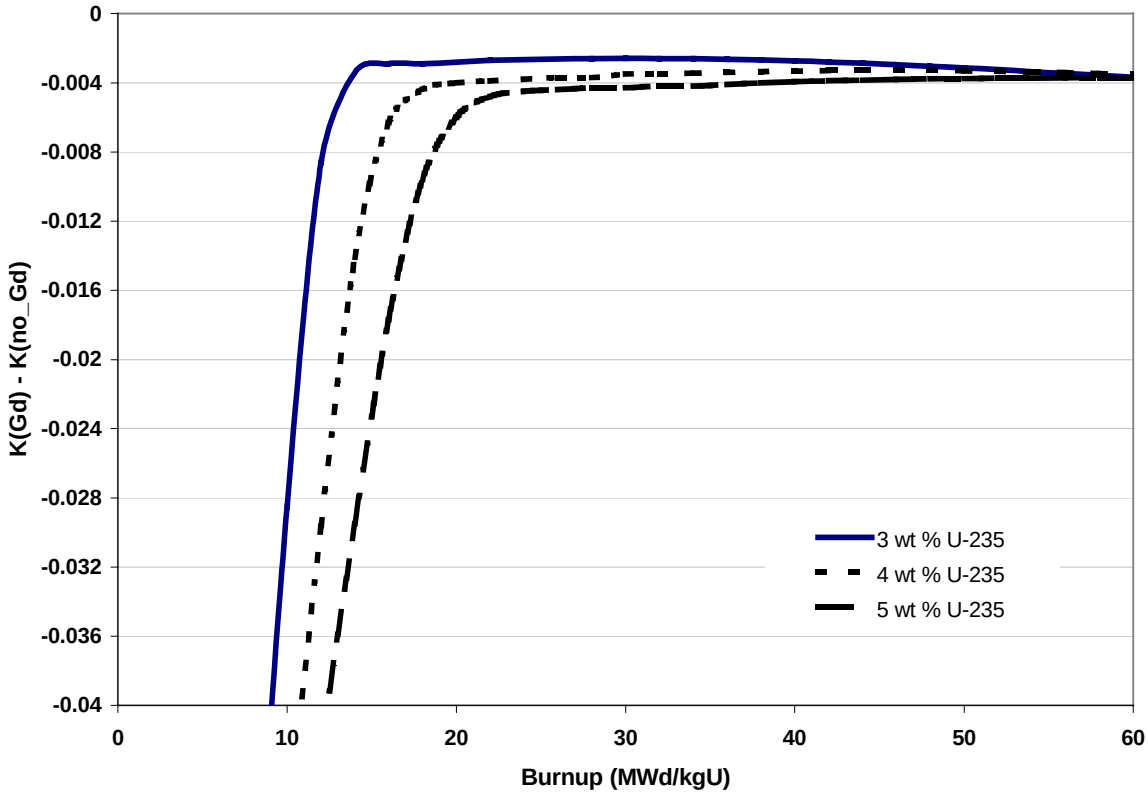

Figure 37 Comparison of Δ*k* values versus burnup with varying gadolinia weight percents. The fuel enrichments are 3.78/3.28 wt % ^{235}U.

The previous calculation, using the integral burnable absorber rods of 6 wt % enriched gadolinia, was further investigated by considering cases with 3, 4, and 5 wt % ^{235}U enrichment. The Δ*k* values for the various enrichments are shown in Figure 38. All of the calculations maintain a negative Δ*k*, and as the ^{235}U enrichment decreases, the Δ*k* decreases. However, the initial ^{235}U enrichment is shown to have a relatively small effect.

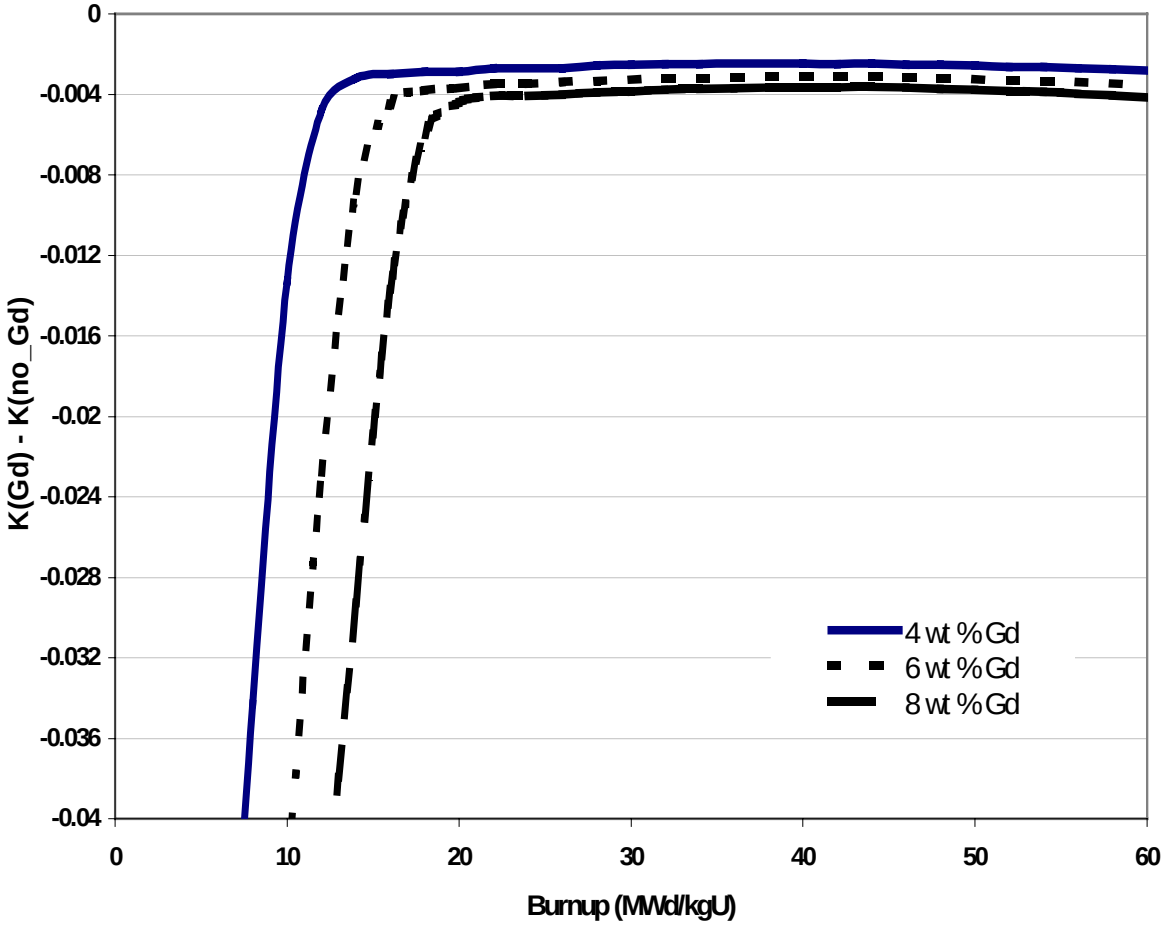

Figure 38 Comparison of Δk values versus burnup with various ^{235}U enrichments. The eight integral burnable absorber rods have 6 wt % Gd_2O_3.

3.3.5.2 Variations of IFBA Loading and Initial Fuel Enrichment

This additional study involves variations in IFBA loading and fuel enrichment in a 17×17 assembly. The dimensions and fuel assembly specifications can be found in Table 2. Analyses were performed for IFBA assembly designs with 32, 64, 80, 104, 128, and 156 IFBA rods and ^{235}U enrichments of 3.0, 4.0, and 5.0 wt %. The dimensions and fuel assembly specifications can be found in Table 2.

The Δk values for the various IFBA loading patterns as a function of burnup for initial ^{235}U enrichment of 4.0 wt % are shown in Figure 39. Consistent with the results shown in Section 3.3.1, the Δk values increase as the number of IFBA rods increase.

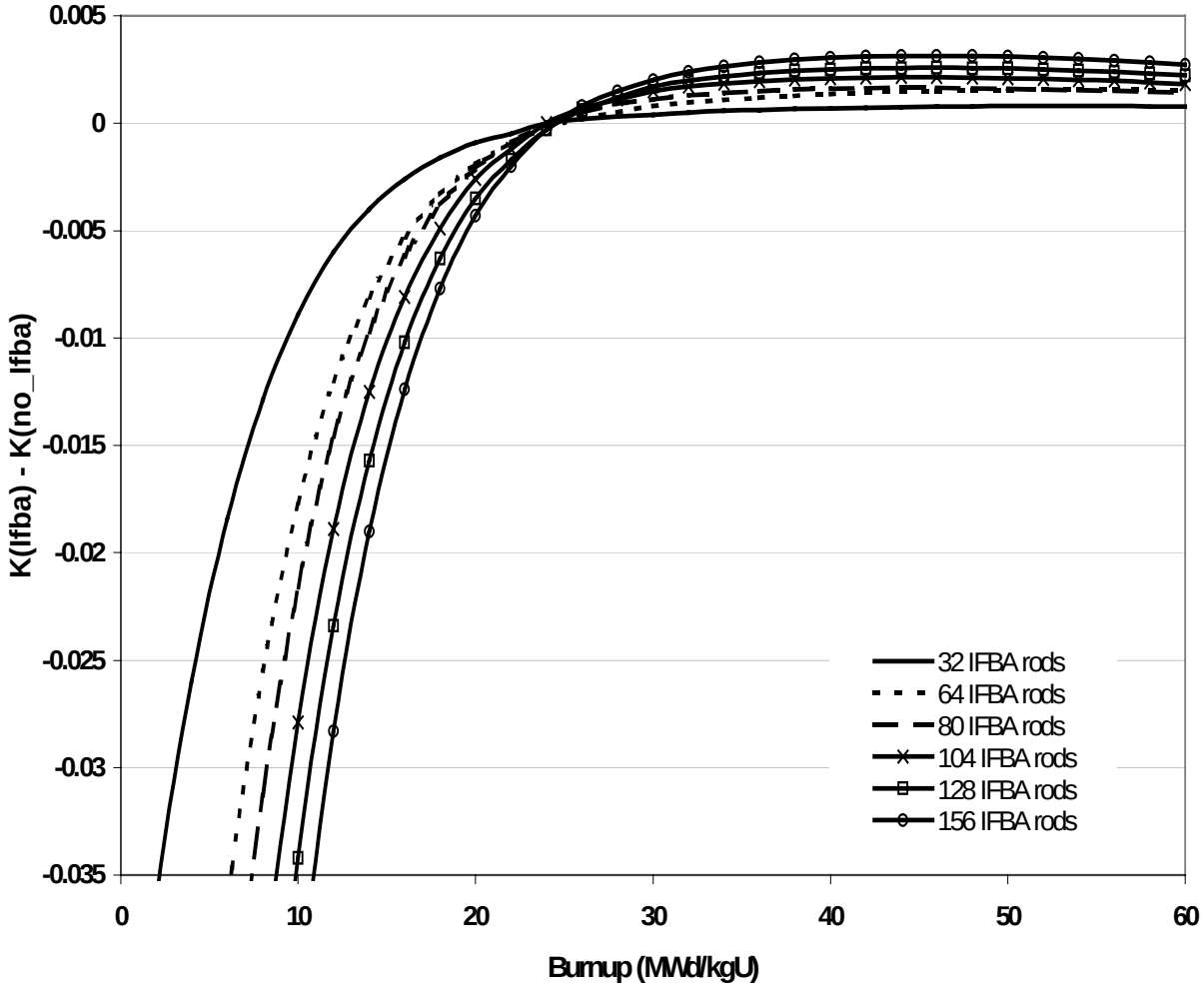

Figure 39 Comparison of Δk values versus burnup with varying IFBA loadings. The ^{235}U enrichment is 4 wt % for all cases.

To illustrate the effect of initial fuel enrichment, Δ*k* values for 3.0, 4.0, and 5.0 wt % ^{235}U are shown in Figures 40 and 41 for IFBA loading patterns of 32 and 156, respectively. Consistent with the results shown in Section 3.3.1, the positive Δ*k* values increase with decreasing enrichment. Note that the 3.0 and 4.0 wt % ^{235}U cases reach a maximum Δ*k* and then begin to decrease.

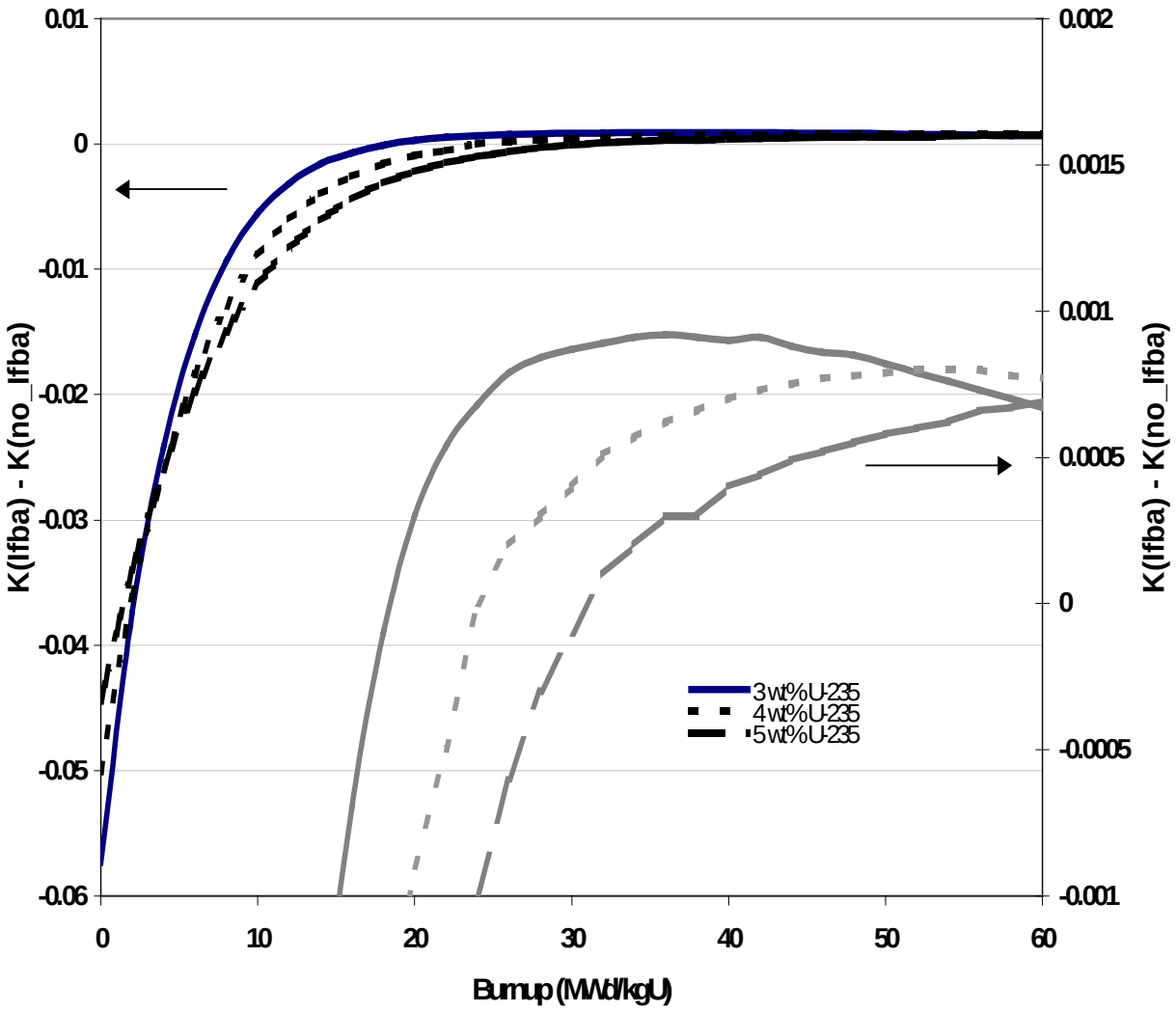

Figure 40 Comparison of Δ*k* values versus burnup with the 32 IFBA loading pattern showing varying ^{235}U enrichments. Note that the results are also plotted on the enlarged scale on the right-hand side y-axis for clarity.

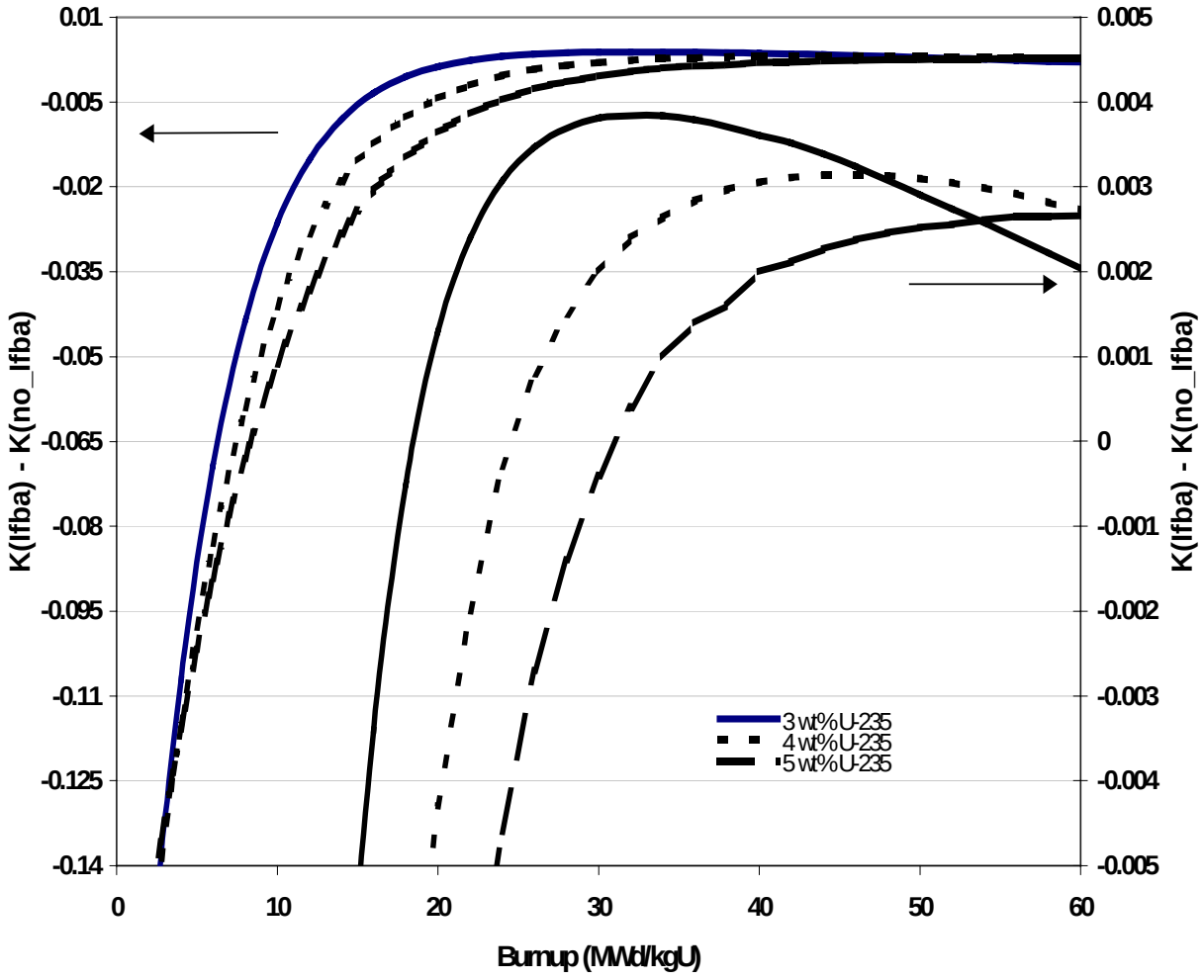

Figure 41 Comparison of Δk values versus burnup with the 156 IFBA loading pattern showing varying ^{235}U enrichments. Note that the results are also plotted on the enlarged scale on the right-hand side y-axis for clarity.

The maximum positive Δ*k* values for the various IFBA cases are summarized in Table 9.

Table 9 Summary of maximum positive Δ*k* values observed for IFBA cases

	Enrichment (wt % ^{235}U)		
IFBA loading pattern	3.0	4.0	5.0
32	0.0009	0.0008	0.0007
64	0.0018	0.0015	0.0013
80	0.0020	0.0016	0.0014
104	0.0026	0.0021	0.0018
128	0.0031	0.0026	0.0022
156	0.0038	0.0031	0.0027

4 SUMMARY AND IMPLICATIONS

Numerous Integral Burnable Absorber (IBA) types have been used in commercial nuclear fuel assembly designs to suppress the initial reactivity. Variations in the IBA poison material, composition, placement within rods, and rod configurations exist among current PWR IBA fuel assembly designs. These IBA characteristics are varied in combination with the initial fuel assembly enrichment and core location to achieve core operating and fuel management goals. To assess the potential impact of these IBAs on the reactivity of SNF, analyses have been presented in this report for IBA types known to the authors. These IBA types include IFBA rods, UO_2-Gd_2O_3 rods, UO_2-Er_2O_3 rods, and Al_2O_3-B_4C rods. Based on the available data, analyses were performed for a representative, realistic range of fuel initial enrichment and poison loading combinations representative of actual assemblies. All IBA types that have been widely used in U.S. commercial PWRs have been included in this evaluation.

Assemblies with IBAs are designed such that the poison material is effectively depleted during the first third of the assembly life. As a result, depending on the IBA type and loading, the assembly reactivity may actually increase with burnup to a maximum or peak where the IBA is essentially depleted. At this point where the IBA is essentially depleted (or beyond), the reactivity of an assembly with IBAs may potentially equal or exceed the reactivity of a nonpoisoned, equivalent enrichment assembly. Therefore, to determine if any of the assemblies with IBAs exceed the reactivity of nonpoisoned, equivalent enrichment assemblies, this evaluation compared k_{inf} values, throughout burnup, between fuel assemblies with and without IBAs. The premise being that if assemblies with IBAs yield lower k_{inf} values (throughout burnup) than assemblies without IBAs, burnup credit criticality safety analyses may conservatively neglect the presence of IBAs. Thus for each unique IBA assembly design considered, a calculation was performed for (1) the actual assembly specification (including the presence of the IBA) and (2) an artificial condition in which the IBA was neglected (non-poisoned, equivalent enrichment case). The difference between the calculated k_{inf} values (Δk) from these two cases was used to assess the reactivity effect of each of the following IBAs types: IFBA rods, UO_2-Gd_2O_3 rods, UO_2-Er_2O_3 rods, and Al_2O_3-B_4C rods.

First, analyses were performed for Westinghouse assembly designs with IFBA rods, including varying numbers of IFBA rods, Boron loadings, and initial fuel enrichments. The results (as a function of burnup) indicate that the k_{inf} values for fuel assemblies containing IFBA rods may exceed the k_{inf} values for fuel assemblies without IFBA rods. In fact, all IFBA assembly designs considered were shown to have a small, positive reactivity effect, as compared to assemblies without IFBA rods. For a fixed initial fuel enrichment, the positive reactivity effect was shown to increase with increasing poison loading (i.e., both increasing ^{10}B loading and increasing number of IFBA rods). Additionally, for a fixed poison loading, the positive reactivity effect was shown to increase with decreasing initial fuel enrichment. For all of the IFBA cases considered, the maximum positive Δk value was found to be 0.4%. However, it should be noted that this maximum value corresponds to a very heavily poisoned, atypical assembly design and, based on the available data, does not appear representative of typical IFBA assemblies. The positive reactivity effect for typical IFBA assembly designs (designs that are used in significant numbers) appears to be less than ~0.3%.

Second, analyses were performed for assembly designs with UO_2-Gd_2O_3 rods, including variations in gadolinia loadings (wt % Gd_2O_3 and number of gadolinia-bearing rods) and initial fuel enrichment. The calculations showed that, throughout burnup, the k_{inf} values for fuel assemblies containing UO_2-Gd_2O_3 rods remain less than the k_{inf} values for fuel assemblies without UO_2-Gd_2O_3 rods. Therefore, it is concluded that gadolinia-bearing rods yield a negative reactivity effect. The negative reactivity effect was found to increase with increasing gadolinia loading (wt % Gd_2O_3 and number of gadolinia-bearing rods) and increasing initial fuel enrichment. For all of the actual fuel assembly designs considered, the k_{inf} values for fuel assemblies with gadolinia-bearing rods were always less (by as much as 0.5%) than the k_{inf} values for fuel assemblies without gadolinia-bearing rods.

Third, analyses were performed for assembly designs with UO_2-Er_2O_3, including variations in the number of UO_2-Er_2O_3 rods. For the assembly designs considered, the k_{inf} values for the non-erbia-bearing fuel assemblies consistently remained higher than the k_{inf} values for the erbia-bearing fuel assemblies. The amount by which the k_{inf} values for the erbia-bearing fuel were less than the k_{inf} values for the non-erbia-bearing fuel increased with increasing numbers of UO_2-Er_2O_3 rods. Therefore, it is concluded that erbia-bearing rods yield a negative reactivity effect.

Finally, analyses were performed for assembly designs with Al_2O_3-B_4C rods, including variations in the number Al_2O_3-B_4C rods. For the assembly designs considered, the k_{inf} values for the fuel assemblies with Al_2O_3-B_4C rods consistently remained lower than the k_{inf} values for the fuel assemblies without Al_2O_3-B_4C rods. The amount by which the k_{inf} values for the fuel assemblies with Al_2O_3-B_4C rods were less than the k_{inf} values for the fuel assemblies without Al_2O_3-B_4C rods increased with increasing numbers of Al_2O_3-B_4C rods. Therefore, it is concluded that Al_2O_3-B_4C rods yield a negative reactivity effect.

In summary, the analyses presented in Section 3 demonstrate that the neutron multiplication factor for an assembly without IBAs is always greater (as a function of burnup) than the neutron multiplication factor for an assembly that utilized any of the following IBA types: UO_2-Gd_2O_3, UO_2-Er_2O_3, or Al_2O_3-B_4C rods. Conversely, the neutron multiplication factor for an assembly with IFBA rods present was found to exceed (maximum of 0.4% Δk) the neutron multiplication factor for an assembly without IFBA rods. Therefore, neglecting the IBAs in a burnup-credit criticality safety analysis will yield conservative results for assembly designs with UO_2-Gd_2O_3, UO_2-Er_2O_3, or Al_2O_3-B_4C IBA rods and non-conservative results for assembly designs with IFBA rods. In all cases, for burnups characteristics of discharge, the reactivity effect of IBAs is relatively small (less than ~1.0% Δk) and generally well behaved.

These results are important to burnup credit because they demonstrate that assembly designs with UO_2-Gd_2O_3, UO_2-Er_2O_3, or Al_2O_3-B_4C IBA rods are less reactive throughout burnup than their corresponding designs without the IBA rods (i.e., non-poisoned, equivalent enrichment). Consequently, with the notable exception of assemblies with IFBA rods, neglecting the presence of IBAs in a burnup credit criticality safety evaluation will yield slightly conservative results. For assembly designs with IFBA rods, the positive reactivity effect must be appropriately addressed.

5 RECOMMENDATIONS

The analyses presented in this report provide a technical basis for revising the current ISG (Ref. 2) to allow burnup credit for assembly designs with Integral Burnable Absorbers (IBAs). Although the analyses do not address the issue of validation of depletion methods for assembly designs with IBAs, they do demonstrate that the effect of the IBAs is relatively small (at or near target discharge burnups) and generally well behaved. Furthermore, the recommended approaches for addressing fuel assemblies with IBAs, as described below, do not involve explicit analyses with IBAs present, and thus do not necessitate validation of the depletion methods for assembly designs with IBAs. Therefore, it is concluded that the effect of the various IBA types may be adequately calculated and that the current restriction on assemblies with IBAs should be eliminated.

The analyses described in this report demonstrate that, with the notable exception of the Westinghouse IFBA rods, the neutron multiplication factor for an assembly without IBAs is always greater (throughout burnup) than the neutron multiplication factor for an assembly with IBAs, including UO_2-Gd_2O_3, UO_2-Er_2O_3, and Al_2O_3-B_4C rods. Therefore, for those IBAs other than IFBAs, burnup credit criticality safety analyses may simply and conservatively neglect the presence of the IBAs by assuming non-poisoned, equivalent enrichment fuel. Considering the variations in IBA assembly designs, neglecting the presence of the IBAs is an important simplifying assumption that does not add significant unnecessary conservatism.

For assembly designs with IFBA rods the neutron multiplication factor was found to be slightly greater (maximum of 0.4% Δk) than the neutron multiplication factor for an assembly without IFBA rods. Therefore, the positive reactivity effect due to the presence of IFBA rods should be considered in any burnup-credit criticality safety analysis seeking to qualify IFBA assemblies as acceptable contents. Due to the significant variations in IFBA assembly designs, simple strategies for addressing the positive reactivity effect are desirable. Two possible strategies for consideration include: (1) the inclusion of a small reactivity bias to bound the effect of the IFBA rods, or (2) demonstration that the effect of the IFBA rods is bounded by the effect of the BPRs. While feasible, the use of a small reactivity bias would likely require justification for the value of the bias, which may result in unnecessary conservatism. Alternatively, it will be simpler and less burdensome to demonstrate that the effect of the IFBA rods is bounded by the BPR modeling approach. Comparison of the reactivity effect of IFBA rods (shown in this report) to the reactivity effect of BPRs, as quantified in a related report (Ref. 1), clearly demonstrates that the reactivity effect of the IFBA rods is significantly less than the reactivity effect due to BPRs. Furthermore, considering the fact that BPRs are seldom used within assemblies that have IFBA rods, and when used, are employed in a limited way (e.g., a small number of BPRs may be used in conjunction with an assembly that has a relatively light IFBA loading), reliance on the BPR modeling to account for the effect of IFBA rods is justified. However, this approach would only be applicable to analyses that consider BPR exposure.

6 REFERENCES

1. J. C. Wagner and C. V. Parks, *Impact of Burnable Poison Rods on PWR Burnup Credit Criticality Safety Analyses for Dry Cask Storage and Transport*, NUREG/CR-XXXX (ORNL/TM-2000/373), U.S. Nuclear Regulatory Commission, Oak Ridge National Laboratory, in preparation.

2. Spent Fuel Project Office Interim Staff Guidance – 8, Rev. 1 – Limited Burnup Credit, U.S. Nuclear Regulatory Commission, July 30, 1999.

3. P. M. O'Leary and M. L. Pitts, "Effects of Integral Burnable Absorbers on PWR Spent Nuclear Fuel," *Trans. Am. Nucl. Soc*. **83**, November 2000.

4. J. J. Casal,R. J. J. Stamm'ler, E. A. Villarino, and A. A. Ferri, "HELIOS: Geometric capabilities of a new fuel-assembly program," Vol. 2, p. 10.2.1 113, *Intl Topical Meeting on Advances in Mathematics, Computations, and Reactor Physics*, Pittsburgh, Pennsylvania, April 28–May 2, 1991.

5. R. J. Cacciapouti and S. Van Volkinburg, "Axial Burnup Profile Database for Pressurized Water Reactors," YAEC-1937, Yankee Atomic Electric Company (May 1997).

6. R. J. Cacciapouti, personal communication, Duke Engineering & Services, September 14, 2000. (More detailed/complete reference to be added before final publication)

7. System Description for Reactor Core for Ulchin 5&6 Nuclear Power Plants, N0696-RE-SD280, KOPEC, 1997.

8. R. J. Cacciapouti, personal communication, Duke Engineering & Services, September 14, 2000. (More detailed/complete reference to be added before final publication)

9. Calvert Cliffs Nuclear Power Plant UFSAR, Rev. 26 Constellation Nuclear.

INTERNAL DISTRIBUTION

1. S. M. Bowman, 6011, MS-6370
2. B. L. Broadhead, 6011, MS-6370
3. W. C. Carter, 6011, MS-6370
4. M. D. DeHart, 6011, MS-6370
5. M. E. Dunn, 6011, MS-6370
6. K. R. Elam, 6011, MS-6370
7. R. J. Ellis, 6025, MS-6363
8. M. B. Emmett, 6011, MS-6370
9. I. C. Gauld, 6011, MS-6370
10. J. C. Gehin, 6025, MS-6363
11. S. Goluoglu, 6011, MS-6370
12. D. F.Hollenbach, 6011, MS-6370
13. C. M. Hopper, 6011, MS-6370
14. B. L. Kirk, 6025, MS-6362
15. M. A. Kuliasha, 6025, MS-6435
16. A. Loebl, 6025, MS-6435
17. S. B. Ludwig, PRI, MS-6495
18. B. D. Murphy, 6011, MS-6370
19. C. V. Parks, 6011, MS-6370
20. L. M. Petrie, 6011, MS-6370
21. R. T. Primm III, 6011, MS-6370
22. C. E. Pugh, 9201-3, MS-8063
23. J.-P. Renier, 6011, MS-6370

24–28. C. E. Sanders, 6011, MS-6370

29. T. E. Valentine, 6025, MS-6362

30–34. J. C. Wagner, 6011, MS-6370

35. R. M. Westfall, 6011, MS-6370
36. Laboratory Records-RC
    4500N, MS-6285
37. Central Research Library
    4500N, MS-6191

38–50. Return extra ORNL copies to:
    W. C. Carter, 6011, MS-6370

EXTERNAL DISTRIBUTION

51. M. L. Anderson, Framatome Cogema Fuels, 1261 Town Center Drive, Las Vegas, Nevada 89134
52. S. Anton, Holtec International, 555 Lincoln Drive West, Marlton, NJ 08053
53. A. C. Attard, U.S. Nuclear Regulatory Commission, NRR/DSSA/SRXB, MS O10-B3, Washington, DC 20555
54. M. G. Bailey, NMSS/SFPO/SLID, U.S. Nuclear Regulatory Commission, MS T8-A23, Washington, DC 20555-0001
55. L. Barrett, Office of Civilian Radioactive Waste Management, RW-232 20545, U.S. Department of Energy, Washington, DC 20545
56. C. J. Benson, Bettis Atomic Power Laboratory, P.O. Box 79, West Mifflin, PA 15122
57. G. H. Bidinger, 17016 Cashell Road, Rockville, MD 20853
58. J. Boshoven, Transnuclear West, Inc., 39300 Civic Center Drive, Suite 280, Fremont, CA 94538
59. M. C. Brady Raap, Battelle, Pacific Northwest National Laboratory, P.O. Box 999 / MS K8-34, Richland, WA 99352
60. R. J. Cacciapouti, Duke Engineering and Services, 400 Donald Lynch Boulevard, Marlborough, MA 01752
61. D. E. Carlson, NMSS/SFPO/TRD, U.S. Nuclear Regulatory Commission, MS O13-D13, Washington, DC 20555-0001

62. J. M. Conde López, Consejo de Seguridad Nuclear, Jefe de Area de Ingeniería Nuclear, Subdirección General de Technologia Nuclear, Justo Dorado, 11, 28040 Madrid, Spain
63. D. R. Conners, Bettis Atomic Power Laboratory, P.O. Box 79, West Mifflin, PA 15122
64. P. Cousinou, Institut de Protection et de Sûreté Nucleaire, Départment de Recherches en Sécurité, CECI B.P. 6 - 92265 Fontenzy-Aux-Roses, Cedex, France
65. W. Davis, Framatome Cogema Fuels, 1261 Town Center Drive, Las Vegas, Nevada 89134
66. T. W. Doering, EPRI, 920 Morning Sun Court, Las Vegas, Nevada 89110
67–71. D. D. Ebert, RES/DSARE/SMSAB, U.S. Nuclear Regulatory Commission, MS T10-K08, Washington, DC 20555-0001
72. F. Eltawila, RES/DSARE/SMSAB, U.S. Nuclear Regulatory Commission, MS T10-E32, Washington, DC 20555-0001
73. R. N. B. Gmal, Gesellschaft für Anlagen-und Reaktorsicherheit (GRS) mbH, Leiter der Gruppe Kritikalität, Forschungsgelände, 85748 Garching b. München
74. P. Grimm, Paul Scherrer Institute, CH-5232 Villigen Psi, Switzerland
75. N. Gulliford, Winfrith Technology Centre, 306/A32, AEA Technology PLC, Winfrith, Dorchester, Dorset DT2 8DH, United Kingdom
76. A. Haghighat, Mechanical and Nuclear Engineering, 137 Reber Building, Pennsylvania State University, University Park, PA 16802
77. S. Hanauer, U.S. Department of Energy, RW-22, Washington, DC 20545
78. G. Harms, Sandia National Laboratory, PO Box 5800, Mail Stop 1143, Albuquerque, New Mexico 87185-1143
79. L. A. Hassler, Framatome Cogema Fuels, 3315 Old Forest Road, P.O. Box 10935, Lynchburg, VA 24506-0935
80. D. Henderson, Framatome Cogema Fuels, 3315 Old Forest Road, P.O. Box 10935, Lynchburg, VA 24506-0935
81. Hae Ryong Hwang, Radiation Safety Analysis Group, KOPEC, 150, Duckjin Dong, Taejon, South Korea 305-600
82. R. A. Knief, XE Corporation (XEC), P.O. Box 90818, Albuquerque, NM 87199
83. H. Kühl, Wissenschaftlich-Technische Ingenieurberatung GMBH, Karl-Heinz-Beckurts-Strasse 8, 52428 Jülich
84. W. H. Lake, Office of Civilian Radioactive Waste Management, U.S. Department of Energy, RW-46, Washington, DC 20585
85. D. B. Lancaster, Nuclear Consultants.com, 320 South Corl Street, State College, PA 16801
86. C. Lavarenne, Institut de Protection et de Sûreté Nucléaire, Department of Prevention and Studies of Accidents, Criticality Studies Division, CEA - 60-68, avenue de Général Leclerc, B.P. 6 - 92265, Fontenay - Aux - Roses, Cedex, France
87. R. Y. Lee, RES/DSARE/SMSAB, U.S. Nuclear Regulatory Commission, MS T10-K8, Washington, DC 20555-0001
88. Willington J. Lee, NAC International, 655 Engineerig Drive, Norcross, GA 30092
89. Y. L. Liu, Argonne National Laboratory, 9700 S. Cass Ave., Bldg.308, Argonne, IL 60439-4825
90. M. Mason, Transnuclear, Two Skyline Drive, Hawthorne, NY 10532-2120
91. A. J. Machiels, Electric Power Research Institute, Advanced Nuclear Technology, Energy Convervation Division, 3412 Hillview Ave., Palo Alto, CA 94304-1395
92. L. Markova, Ustav jaderneho vyzkumu Rez, Theoretical Reactor Physics, Nuclear Research Institute, Czech Republic, 25068 REZ

93. Daniel MARLOYE, Belgonucléaire, Av. Ariane 4, B-1200, Brussels, Belgium
94. C. W. Mays, Framatome Cogema Fuels, 3315 Old Forest Road, P.O. Box 10935, Lynchburg, VA 24506-0935
95. N. B. McLeod, JAI Corporation, 4103 Chain Bridge Road, Suite 200, Fairfax, VA 22030
96. D. Mennerdahl, E. Mennerdahl Systems, Starvägen 12, S-183 57 Täby, Sweden
97. Dr. Raymond L. Murray, 8701 Murray Hill Drive, Raleigh, NC 27615
98. K. A. Neimer, Duke Engineering & Services, 400 S. Tyron St., WC26B, P.O. Box 1004, Charlotte, NC 28201-1004
99. P. Noel, Framatome Cogema, 1261 Town Center Drive, Las Vegas, Nevada
100. I. Nojiri, Japan Nuclear Cycle Development Institute, Environment and Safety Division, Tokai Works, Muramatsu Tokai-mura, Naka-gun Ibaraki-ken 319-1194, Japan
101. J. C. Neuber, SIEMENS AG, KWU NS-B, Berliner Str. 295-303, D-63067 OFFENBACH AM MAIN, Germany
102. A. Nouri, OECD/NEA Data Bank, Le Seine-Saint Germain, 12 Boulevard des Iles, F-92130 Issy-les-Moulineaux, France
103–104. Office of Scientific and Technical Information, U.S. Department of Energy, P.O. Box 62, Oak Ridge, TN 37831
105. Office of the Assistant Manager for Energy Research and Development, Department of Energy Oak Ridge Operations (DOE-ORO), P.O. Box 2008, Oak Ridge, TN 37831
106. H. Okuno, Japan Atomic Energy Research Institute, Department of Fuel Cycle, Safety Research, 2-4 Shirakata-Shirane, 319-1195 Tokai-mura, Naka-Gun, Ibaraki-ken, Japan
107. P. M. O'Leary, Framatome Technologies, 3315 Old Forest Road, P.O. Box 10935, Lynchburg, VA 24506-0935
108. N. L. Osgood, U.S. Nuclear Regulatory Commission, Office of Nuclear Materials Safety and Safeguards, MS O13-D13, Washington, DC 20555-0001
109. O. Ozer, Electric Power Research Institute, 3412 Hillview Ave., Palo Alto, CA 94304
110. T. Parish, Department of Nuclear Engineering, Texas A & M University, College Station, TX 77843-3313
111. V. A. Perin, NMSS/DWM/HLWB, U.S. Nuclear Regulatory Commission, MS T7-F3, Washington, DC 20555-0001
112. B. Petrovic, Westinghouse Electric Company, Science and Technology Department, 1344 Beulah Road, Pittsburgh, PA 15235
113. J. S. Philbin, Sandia National Laboratory, PO Box 5800, Mail Stop 1143, Albuquerque, New Mexico 87185-1143
114. M. Rahimi, NMSS/DWM/HLWB, Office of Nuclear Material Safety and Safeguards, MS T7-F3, Washington, DC 20555-0001
115. E. L. Redmond II, Holtec International, 555 Lincoln Drive West, Marlton, NJ 08053
116. C. Rombough, CTR Technical Services, Inc., 5619 Misty Crest Dr., Arlington, TX 76017-4147
117. D. Salmon, Framatome Cogema, 1261 Town Center Drive, Las Vegas, Nevada 89134
118. A. Santamarina, Commissariat A L'Energie Atomique, Nuclear Reactor Division, Reactor Studies Department, Reactor and Cycle Physics Service, CEA/CADARACHE/DRN/DER/SPRC Bat. 230, 13108 Saint-Paul-Lez-Durance, Cedex, France
119. E. Sartori, OECD/NEA Data Bank, Le Seine-Saint Germain, 12 Boulevard des Iles, F-92130 Issy-les-Moulineaux, France

120. Joe J. Sapyta, Framatome Cogema Fuels, 3315 Old Forest Road, P.O. Box 10935, Lynchburg, Virginia 24506-0935
121. H. H. Schweer, Bundesamt fuer Strahlenschutz, Willi Brandt Str. 5, D-38226 SALZGITTER, Germany
122. G. Sert, Institut de Protection et de Surete Nuclear, Department de Securite des Matieres Radioactives, B.P. 6 - 92265, Fontenay - AUX - Roses, Cedex France
123. D. N. Simister, Health and Safety Executive, Nuclear Installations Inspectorate, St. Peter's House, Balliol Road, Bootle, Merseyside L20 3LZ
124. M. Smith, Virginia Power Co., P.O. Box 2666, Richmond, VA 23261
125. N. R. Smith, AEA Technology, A32 Winfrith, Dorchester, Dorset DT2 8DH, United Kingdom
126. T. Suto, Power Reactor and Nuclear Fuel Development Corporation, Technical Service Division, Tokai Reprocessing Plant, Tokai Works, Tokai-Mura, Naka-gun, Ibaraki-ken, Japan
127. H. Taniuchi, Kobe Steel, Ltd., 2-3-1 Shinhama, Arai-Cho, Takasago, 676 Japan
128. D. A. Thomas, Framatome Cogema, 1261 Town Center Drive, Las Vegas, Nevada 89134
129. P. R. Thorne, British Nuclear Fuels plc (BNFL), Nuclear and Radiological Safety, R101 Rutherford House, Risley Warrington WA3 6AS, United Kingdom
130. J. R. Thornton, Duke Engineering & Services, 230 S. Tyron St., P.O. Box 1004, Charlotte, NC 28201-1004
131. S. E. Turner, HOLTEC International, 230 Normandy Circle East, Palm Harbor, FL 34683
132. M. E. Wangler, U.S. Department of Energy, EH-33.2, Washington, DC 20585-0002
133. A. Wells, 2846 Peachtree Walk, Duluth, GA 30136
134. B. H. White, NMSS/SFPO/TRD, U.S. Nuclear Regulatory Commission, MS O13-D13, Washington, DC 20555-0001
135. Robert Wilson, Rocky Flats Field Office, USDOE, 10808 Highway 93, Golden, CO 80403-8200
136. C. J. Withee, NMSS/SFPO/TRD, U.S. Nuclear Regulatory Commission, MS O13-D13, Washington, DC 20555-0001

NRC FORM 335 (2-89) NRCM 1102 3201, 3202

U.S. NUCLEAR REGULATORY COMMISSION

BIBLIOGRAPHIC DATA SHEET

(See instructions on the reverse)

1. REPORT NUMBER (Assigned by NRC, Add Vol., Supp., Rev., and Addendum Numbers, if any.)

NUREG/CR-
ORNL/TM-2000/321

2. TITLE AND SUBTITLE

Impact of Integral Burnable Absorbers on PWR Burnup Credit Criticality Safety Analysis for Dry Cask Storage and Transport

3. DATE REPORT PUBLISHED

MONTH	YEAR
	2001

4. FIN OR GRANT NUMBER

W6479

5. AUTHOR(S)

C. E. Sanders and J. C. Wagner

6. TYPE OF REPORT

Technical

7. PERIOD COVERED ***(Inclusive Dates)***

8. PERFORMING ORGANIZATION — NAME AND ADDRESS ***(If NRC, provide Division, Office or Region, U.S. Nuclear Regulatory Commission, and mailing address; if contractor, provide name and mailing address.)***

Oak Ridge National Laboratory
Managed by UT-Battelle, LLC
Oak Ridge, TN 37831-6370

9. SPONSORING ORGANIZATION — NAME AND ADDRESS ***(If NRC, type "Same as above"; if contractor, provide NRC Division, Office or Region, U.S. Regulatory Commission, and mailing address.)***

Division of Systems Analysis and Regulatory Effectiveness
Office of Nuclear Regulatory Research
U.S. Nuclear Regulatory Commission
Washington, DC 20555-0001

10. SUPPLEMENTARY NOTES

D. D. Ebert, NRC Project Manager

11. ABSTRACT ***(200 words or less)***

The Interim Staff Guidance on burnup credit issued by the Nuclear Regulatory Commission's Spent Fuel Project Office restricts the use of burnup credit to assemblies that have not used burnable absorbers. This restriction eliminates a large portion of the currently discharged spent fuel assemblies from cask loading, and thus, severely limits the practical usefulness of burnup credit. This report examines the effect of integral burnable absorbers (IBAs) on reactivity to provide technical justification for relaxing the current restriction for dry cask storage and transport, and subsequently, to develop the necessary guidelines for relaxing the current restriction. The effect of IBAs on reactivity for various IBA designs and exposure conditions is shown and discussed. Further, the reactivity effect of IBAs for typical initial fuel enrichment and absorber loadings is quantified as a function of burnup. The report concludes with a discussion on the issues for consideration and preliminary recommendations for inclusion of spent fuel assemblies with IBAs in criticality safety analyses using burnup credit for dry cask storage and transport.

12. KEY WORDS/DESCRIPTORS ***(List words or phrases that will assist researchers in locating the report.)***

criticality safety, burnup credit, transportation, dry storage, integral burnable absorbers

13. AVAILABILITY STATEMENT

unlimited

14. SECURITY CLASSIFICATION

(This Page) unclassified

(This Report) unclassified

15. NUMBER OF PAGES

16. PRICE